Field-scale fault reactivation experiments by fluid injection highlight aseismic leakage in caprock analogs: Implications for CO2 sequestration

Yves Guglielmi, Christophe Nussbaum, Frédéric Cappa, Louis de Barros, Jonny Rutqvist, Jens Birkholzer

International Journal of Greenhouse Gas Control 111 (2021) 103471

Contents lists available at ScienceDirect

International Journal of Greenhouse Gas Control

journal homepage: www.elsevier.com/locate/ijggc

Review article

Field-scale fault reactivation experiments by fluid injection highlight aseismic leakage in caprock analogs: Implications for CO_2 sequestration

Yves Guglielmi [a,*], Christophe Nussbaum [b], Frédéric Cappa [c,d], Louis De Barros [c], Jonny Rutqvist [a], Jens Birkholzer [a]

[a] Energy Geosciences Division, Lawrence Berkeley National Laboratory, Berkeley, CA, United States
[b] Federal Office of Topography, Swisstopo, St-Ursanne, Switzerland
[c] Université Côte d'Azur, CNRS, Observatoire de la Côte d'Azur, IRD, Géoazur, Sophia Antipolis, France
[d] Institut Universitaire de France, Paris, France

ARTICLE INFO

Keywords:
Caprock
Fault
Fluid injection
Induced seismicity
Leakage
Field scale experiments

ABSTRACT

Observations on tens-of-meter scale experiments of fault activation by fluid injection conducted in shales allow exploring how aseismic and seismic events may jeopardize the integrity of a sealing caprock overlying a CO_2 sequestration reservoir. We contrast the behavior of shale faults with another set of experiments conducted in carbonates. Significant fluid leakage occurs along the initially low-permeability shale faults when rupture is activated. Most of the leakage pathway closes when fluid injection ceases and fluid pressure drops. Dilatant slip on the fault plane alone does not explain the observed leakage behavior, which is also caused by fault opening favored by the softness of the shale, and by the structure of the fault zone that prevents fluids from diffusing into the adjacent damage zone. Experiments show a large amount of aseismic deformation. Small-magnitude seismicity ($M_w < -2.5$) is observed outside the pressurized leakage patch. Stress transferred from this aseismic deformation patch can build up to stress-criticality and favor seismicity. Thus, in terms of fault activation in caprocks, aseismic fault slip leading to increased permeability and a loss of seal integrity is of great concern.

1. Introduction

For carbon capture and geological storage (CCS) to become a viable emissions reduction and climate mitigation strategy, the world will need to sequester carbon dioxide (CO_2) in the deep subsurface at an unprecedented scale. A recent global projection by the Global CCS Institute (2020) estimates that around 5.6 gigatonnes (Gt) of CO_2 will need to be captured and stored annually by 2050 – a more than hundredfold increase from today. To achieve these levels, the number of industrial-scale geological sites will have to increase to several thousand worldwide, each of which will require decades-long injection of CO_2 at levels of hundreds of thousands to a few million tonnes per year (IPCC, 2018). Depending on the regional storage capacity of saline aquifers, such an amount of industrial CO_2 storage may cause basin-scale fluid pressurization of up to several tens of bars, which raises questions about storage integrity and induced seismicity (Birkholzer and Zhou, 2009; Birkholzer et al., 2015). Such concerns are related to the potential for triggering notable (felt) or even damaging seismic events, knowing that the risk of such events to occur increases with reservoir pressure and with the injected volumes (Nicol et al., 2011; McGarr, 2014). Indeed, we may refer to another subsurface activity involving injection of large volumes of fluid as an analog for the future of CCS: the large-scale waste water injections occurring in a deep Oklahoma Basin reservoir have triggered several earthquakes exceeding M_w 5.0 (Keranen et al., 2014). Such analog studies tend to show that the large earthquakes would rather occur below the injection interval, often in the crystalline basement (Verdon and Stork, 2016; Keranen and Weingarten, 2018). Vilarrasa and Carrera (2015) suggested that this is because of the larger deviatoric stress and the potential occurrence of large faults hydraulically connected or not to the injection zone. Zoback and Gorelick (2012) pointed to another concern related to large-scale pressurization and induced seismicity. They claimed that small to moderate earthquakes triggered at approximately the CO_2 storage depth could jeopardize the integrity of the seals (or caprocks) overlying the storage formation, as slip or opening of existing, perhaps unidentified faults in these seals can lead to permeability enhancement and eventually leakage of CO_2.

Submitted to International Journal of Greenhouse Gas Control.
* Corresponding author.
E-mail address: yguglielmi@lbl.gov (Y. Guglielmi).

https://doi.org/10.1016/j.ijggc.2021.103471
Received 8 May 2021; Received in revised form 17 August 2021; Accepted 18 September 2021

Earthquakes related to fluid injections have been observed worldwide. Some examples concern CO_2 geological storage (Payre et al., 2014; Kaven et al., 2015; White and Foxall, 2016) or gas and hydrocarbon exploitation (Bardaine et al., 2008). In this paper, we focus on this confirmed risk of induced seismicity generating permeable pathways in caprocks.

Theoretical papers based on fully coupled hydromechanical numerical modeling tend to show that even if a fault in a shale formation undergoes seismic slip, leakage through a caprock is unlikely to occur at a significant level because of (1) the high ductility of such typically clay-rich faults (Vilarrasa and Makhnenko, 2017) and (2) the heterogeneous nature of faults intersecting multilayered shale/sandstone sequences (Rutqvist et al., 2016). However, as demonstrated at the laboratory scale, gas injection into shale samples can create discrete dilatant pathways associated with a localized pressurization of a fault-type discontinuity (Cuss and Harrington, 2016). It was furthermore shown that such discrete leakage and slip is possible without any observable fault reactivation, whatever the orientation of the fault towards stress (Cuss et al., 2015). And at the field scale, the observation of natural seeps proves that faults can allow for complex upward migration of CO_2 (Nicol et al., 2017). It appears that the underlying science related to fault reactivation and CO_2 leakage through faulted caprocks is not well understood. Many questions remain—such as how such pathways can be created in initially low permeable fault zones, whether they may fully extend across the caprock, how long will they remain permeable, and what are the expected leakage rates—in particular when considering major industrial-scale projects with long-term large-scale pressure buildup.

Laboratory scale tests performed at the centimeter scale hardly represent the complexity of an often several meter thick and compartmentalized fault zone, and obviously cannot reproduce large magnitude induced earthquakes. Industrial sites provide "empirical" insights but under operational constraints that intrinsically limit the control of the experimental conditions despite the pioneering work by Raleigh et al. (1976). In contrast, *in situ* experiments at the tens-of-meter scale allow controlled activation of pre-existing faults by fluid injection, provide access to the complex architecture of the entire fault, and with high-resolution monitoring in place offer an opportunity for tracking fault slip and induced seismicity close to the nucleation zone. Amann et al. (2018) conducted fault reactivation experiments in deep crystalline rocks at the Grimsel site (Switzerland) in order to study the seismic-hydromechanical behavior of faults during deep geothermal reservoir stimulations. Few such experiments have recently been conducted in reservoir- and in caprock analogues to study the relationship between fault leakage and induced seismicity (Guglielmi et al., 2015a; Michael et al., 2019; Zappone et al., 2021). The key idea is to pressurize a sealed section of a borehole intersecting a fault zone by injecting a fluid (i.e., pure water or a CO_2-in-brine solution) in order to trigger millimeter-scale slip by lowering the effective normal stress acting on the fault. As an example, the experimental design of the meso-scale experiments described in Guglielmi et al. (2015a) is a setup with an injection borehole crossing the entire fault zone and a number of monitoring boreholes nearby (Fig. 1). The section of the injection borehole that intersects the fault is isolated by two inflatable packers and contains a high-resolution probe (the SIMFIP probe) that allows the continuous monitoring of three-dimensional displacements of the fault synchronously with injection pressure and flowrate (Guglielmi et al., 2014). The monitoring boreholes may be instrumented with a similar SIMFIP probe and with different types of seismic sensors. A typical activation experiment consists of increasing the pressure step-by-step in the injection zone until fault slip is triggered. When fault is at slip, pressure is maintained for several minutes to study the relationships between slip, opening, permeability variations and induced micro-seismicity. All instruments are synchronized and permanently monitor during the entire experiment.

Here, we compare several controlled-injection fault reactivations

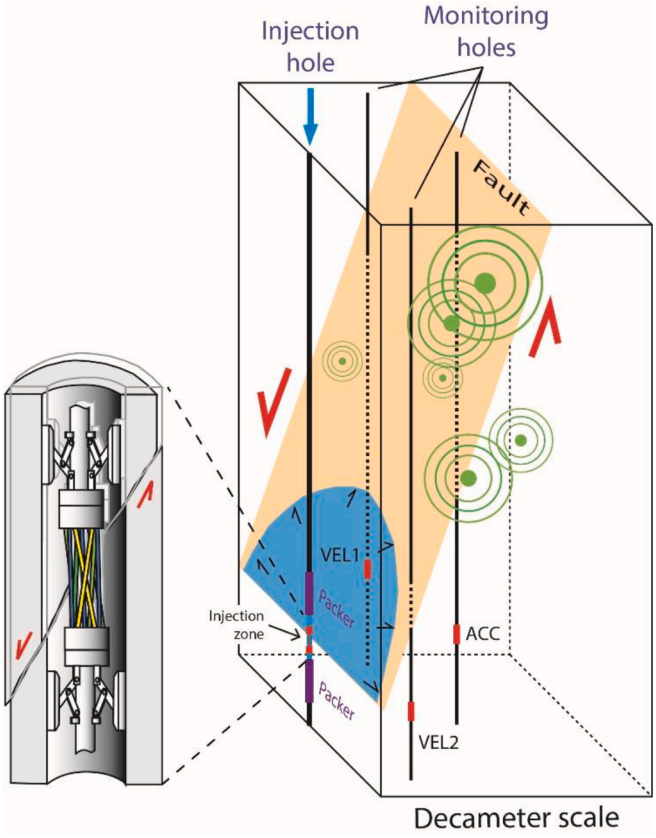

Fig. 1. Fault activation experiment concept caused by fluid injection. Block diagram on the right shows the typical fault activation setting (modified from Guglielmi et al., 2015a). Green circled schematically represent seismic events. Blue half circle figures the pressurized fault patch. The three-dimensional SIMFIP fault displacement sensor is shown on the left (not to scale). This sensor is a deforming cage that records fault movements while being clamped on each of the fault compartment. VEL1, VEL2 and ACC are seismic sensors. (For interpretation of the references to color in this figure legend, the reader is referred to the web version of this article.)

that our group conducted in the Opalinus Clay in the Mont Terri Underground Research Laboratory (URL) in Switzerland and in the Tournemire Clay in France, which are both caprock analogs. We discuss characteristics and findings from these shale fault experiments in comparison with a set of similar fault activation experiments conducted in a porous Cretaceous carbonate reservoir (LSBB, France). The carbonate reservoir fault serves as an analog for the reservoir rocks potentially used for CO_2 storage. All fault activations were conducted using the same protocol of controlled fluid injection while monitoring fault displacements, pore pressure and micro-seismicity in the nearfield (meter-to-few meters) of the injection source. At one given site, we usually conduct several injections, in order to probe different locations in the fault zone (by moving the probe in the injection borehole), to explore the effects of different injection duration from several minutes to a few days, or to examine different injection protocols from a pressure-controlled to a flow-rate-controlled injection type. In total, we performed six different experiments at Tournemire, five at Mont Terri and twelve at LSBB. The tested faults are under a similar normal stress value of 2 to 5 MPa at a depth of about 300-to-500 m that allows focusing on the processes leading to induced seismicity, and to relate seismicity to differences in hydromechanical activation behavior (Tables 1 and 2). One obvious difference is that the carbonate reservoir fault displays a significant initial $\sim 7 \times 10^{-12}$ m^2 permeability (Guglielmi et al., 2015a) while the shale caprock faults displays a low initial permeability of $\sim 10^{-16}$ to 10^{-19} m^2 that may be as low as the permeability of the intact shale

Table 1
Properties of the activated faults. Mont Terri fault properties come from Jeanne et al. (2018) and Wenning et al. (2021) for the permeability and from Orellana et al. (2019) for friction. LSBB fault properties come from Guglielmi et al. (2015a) for permeability and from Cappa et al. (2019) for friction. Tournemire fault properties come from Guglielmi et al. (2015b) for permeability and static friction (a and b frictional values come from unpublished experimental data).

Site	Date of Experiment	Fault Dip dir. (°)	Dip (°)	Friction μ_s	(a – b) Min	Max	Initial Permeability (K_{h0}) (m^2)	Activation Pressure (MPa)
Mont Terri (Switzerland)	2015 2020	140	60	0.4 to 0.5	0.002	0.013	6×10^{-17} to 10^{-19}	5.95
LSBB (France)	2011 and 2015	300	70	0.67	−0.01	0.006	7×10^{-12}	1.5
Tournemire (France)	2014	260	80	0.47	0.003	0.015	$2 - 5 \times 10^{-16}$	3.3 – 3.4

Table 2
Stress state and slip tendency at the three test sites. Stress estimations come from Guglielmi et al. (2020b) for Mont Terri, Guglielmi et al. (2015a) and Duboeuf et al. (2021) for LSBB, Cornet (2000) and Guglielmi et al. (2015b) for Tournemire.

Site	σ_1 Dip Dir / Dip /Magnitude (dd/d/M) dd/d (°)	(MPa)	σ_2 Dip Dir / Dip /Magnitude (dd/d/M) dd/d (°)	(MPa)	σ_3 Dip Dir / Dip /Magnitude (dd/d/M) dd/d (°)	(MPa)	σ_n (MPa)	τ (MPa)	Slip Tendency $\frac{\tau}{(\sigma_n - P_f)}$
Mont Terri (Switzerland)	-/90 ± 10°	5.5 ± 0.1	310/0 ± 10°	4.7 ± 0.1	40/0 ± 10°	3.8 ± 0.1	4.9	0.4	0.12
LSBB (France)	-/80 ± 10°	6 ± 0.4	110/0 ± 10°	5 ± 0.4	200/0 ± 10°	3 ± 0.4	4.4	1.1	0.38
Tournemire (France)	162/0 ± 10°	4 ± 2	72/82 ± 10°	3.8 ± 0.4	72/8 ± 10°	2.1 ± 1	2.1	0.3	0.41

(Nussbaum and Bossart, 2004; Yu et al., 2017; Jeanne et al., 2018; Wenning et al., 2021). Here, we discuss how such controlled-injection field experiments help better understand how faults may reactivate in a caprock overlying a CO_2 storage reservoir and how the reservoir pressure buildup may eventually generate induced seismicity. We first compare the geological characteristics of faults in shale layers compared to those in reservoirs. Second, we discuss how leakage flowpaths can be created in these faults, highlighting the tight link between fault rupture and leakage. Third, we analyze if and how this leakage activation is related to induced seismicity and where such seismicity may occur. Fourth, we provide some insights into partial post-activation self--sealing. Finally, we discuss how such experiments, by bridging laboratory and reservoir scales, may help to assess the risk for caprock leakage from pressure-driven fault slip in industrial CCS projects.

2. Observations from controlled experiments in reservoir-caprock analogues

The fault reactivation experiments discussed in this study have been conducted at three different sites and in three different rock types (Fig. 2). The three sites are all located several hundred meter deep adjacent to tunnels within underground research facilities. These facilities provide experimental space close to the subsurface fault systems allowing for dense monitoring of the fault activation behavior. In all experiments, the activated fault segments are initially seismically inactive before injection (i.e., low tectonic strain). Key characteristics of the three separate sites are as follows: with mineralogy defined in terms of the ternary mixtures of tectosilicates (Si), carbonates (Ca) and phyllosilicates (Cl) as shown in Fig. 2.

The Mont Terri Main Fault (Fig. 2a) is a shale fault (Si/Ca/Cl = 20/

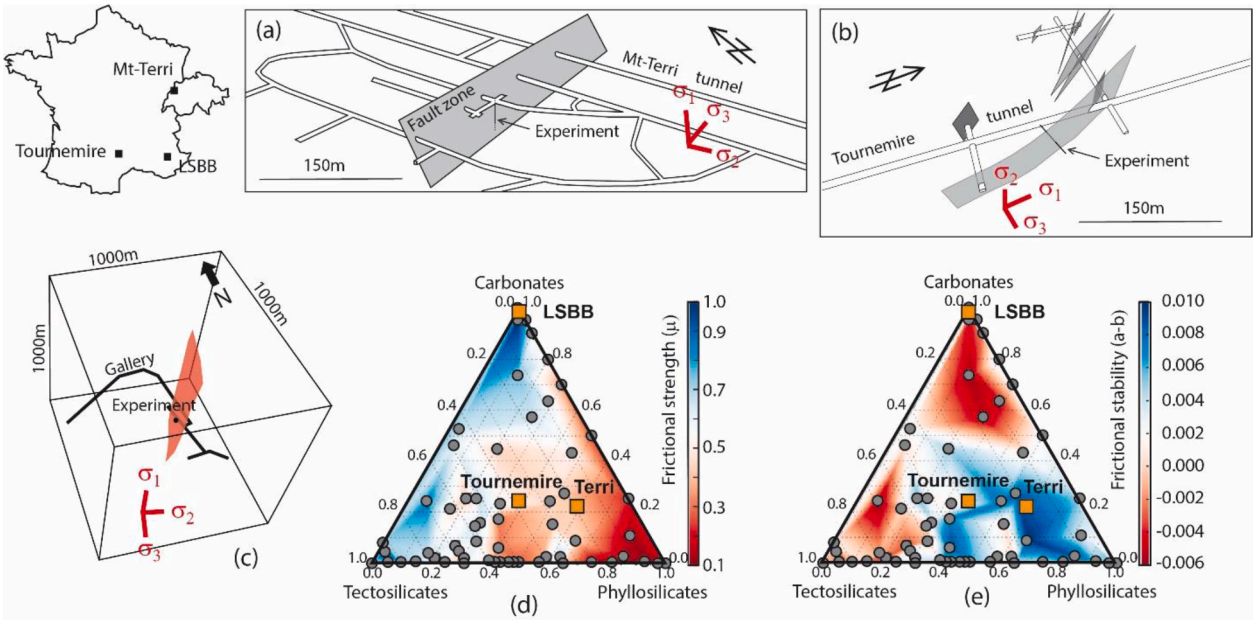

Fig. 2. Geological setting of different experiments of fault activation by fluid injection in Underground Research Laboratories (URL); (a) Mont Terri URL Main Fault experiment at 350 m depth; (b) Tournemire URL experiment at 250 m depth; (c) LSBB URL at 300 m depth; (d) Activated average faults friction coefficient and (e) rate-and-state frictional stability plotted as a function of mineralogy. Gray dots are source data from laboratory tests performed at different slip velocities ranging from 0.01 to 300 μm/s. Figures d and e are modified from Fang et al. (2018) where experimental details can be found. Note the contrasting mineralogy and state of stresses of the three fault reactivation experiments.

22/58%). It is a kilometer N69°−47°E thrust cutting the Opalinus Clay formation (Aalenian) which is considered a moderately indurated clay formation (Mazureck et al., 2008). The fault is a 0.8-to-3 m wide highly deformed zone composed of fault gouge, shear bands, meso-scale folds, microfolds, numerous fault planes and apparent undisturbed parts. Core observations show that almost all of the fault planes strike and dip belong to the same directional family striking N040°-to-N060° dipping 35-to-65° SE. It is connected to the Jura deep decollement structures and it can be interpreted as a shear fault-bend fold (Nussbaum et al., 2011). The fault-bend fold passively steepens from 20° to around 40°−45° in sequence with the folding of the Mont Terri anticline. The fault shear offset is ~10 m. Fault initial permeability is 6×10^{-17} to 10^{-19} m^2 (Table 1). The experiment took place in vertical boreholes crosscutting the fault at ~350 m depth. Water injections were consecutively conducted in five straddle-packer intervals set across different fault structures. Given the range of ambient pore pressures of ~2 MPa and the current state of stress (Fig. 2a and Table 2) the fault tendency to slip is low (0.12 in Table 2). Thus, the fault and most of the features contained in the fault zone are not optimally oriented versus stress for shear slip activation.

The Tournemire Fault is shale fault (Si/Ca/Cl = 38/24/38%, Fig. 2b). It is a N0°−70-to-80°W anticlockwise strike slip fault cutting the Toarcian shale which is considered a highly indurated and fractured formation (Lefevre et al., 2016; Mazureck et al., 2008). The fault length is >300 m being part of a complex km-scale fault network. Fault offset is ~10 m and fault thickness is 8-to-10 m. The fault architecture is characterized by a 0.85-to-2.4 m thick fault core and a dissymmetric fractured damage zone containing the following fracture families strike and dip: (1) N110-to-140, 50°N-or-S, (2) N160, 20-to-40°W and (3) N0-to-10, 70-to-80°W. The two first families display significant calcite fillings while the third one is characterized by lustrated striated planes that may occasionally contain thin gouge material. The fault core displays significant heterogeneity characterized by cataclastic zones of varying thicknesses from 0.4 to 0.01 m intercalated with thin 0.1-to-0.2 m highly fractured zones. The complex fault zone architecture is related to multi-phase activations of the fault under two main tectonic stress regimes: normal faulting during Upper Jurassic to Lower Cretaceous followed by sinistral strike slip reactivation during the Eocene– Pyrenean compression. Fault initial permeability is $2 - 5 \times 10^{-16}$ m^2 (Table 1). The experiment took place in eight subhorizontal boreholes crosscutting the fault at ~350 m depth. Water injections were consecutively conducted in five straddle-packer intervals set across different fault structures. Given the range of ambient pore pressures of ~0.8 to 1.5 MPa and the current state of stress (Fig. 2b and Table 2) the fault tendency to slip is relatively high (0.42 in Table 2). Thus, the fault is close to the critical state for strike-slip fault shear activation.

The LSBB fault is a carbonate fault (Si/Ca/Cl = <5/100/<5%). It is at least ~500 m long and trends N030–70°W (Jeanne et al., 2012). It cuts through low-dipping grainstone carbonate layers of 5-to-15% porosity (Cretaceous inner platform Rudists' rich facies), with strike-slip-to-normal cumulated offset of a few meters. The fault zone consists of sub-parallel fractures of 1–10 m length and discontinuous thin breccia. The fault is a late-Cretaceous extensional structure reactivated during the Miocene-to-Pliocene Alpine compression phase. It is located in the unsaturated zone of the LSBB carbonates where the current state of stresses makes the fault close to critical state for normal slip (Fig. 2c and Table 2). Fault initial permeability is $7\ 10^{-12}$ m^2 (Table 1), which is much higher than the initial permeability in the Mont Terri and Tournemire faults. As a reminder, we are studying the carbonate fault as an analog for a reservoir fault in contrast to a shale fault. Given the current state of stress (Fig. 2c and Table 2), the fault tendency to slip is relatively high (0.38 in Table 2). Thus, the fault is close to the critical state for normal-slip fault shear activation.

Laboratory tests on samples from the three sites show a large variability of the friction coefficients μ_s from 0.4 to 0.7, respectively between clay rich and carbonate sites (Fig. 2 and Table 1, Cappa et al., 2019; Orellana et al., 2019). It is no surprise that the clay-rich faults display a much lower frictional coefficient than the carbonate rich faults. In addition, clay-rich faults display a positive (a – b) value while the carbonate rich faults display a null-to-negative value for similar slow slip velocities of micron to several microns per second. Both clay and carbonate fault frictional properties were measured using the biaxial rock deformation apparatus BRAVA (Brittle-Rock investigation Apparatus) installed at INGV (Istituto Nazionale di Geofisica e Vulcanologia, Roma) set in a direct shear configuration (Collettini et al., 2014). The (a – b) value characterizes the variations of frictional shear strength due to its dependence on slip rate and on the evolving properties of the contact population between the two surfaces of a shear zone (rate-and-state friction models, see Dieterich, 1979, 1981 and Ruina, 1983 for details). A negative value shows that friction decreases with slip rate, which may potentially lead to dynamic instability and seismic rupture. A positive value indicates that friction increases with slip rate, thus towards slip stability and aseismic rupture of the fault. Fig. 2 thus suggests that clay-rich faults have a tendency towards stable (rate strengthening behavior) rupture, and this correlates to their mineralogy. In contrast, carbonate rich faults have a tendency towards unstable rupture (rate weakening behavior). Table 1 shows that the Mont Terri and LSBB faults are typical examples of these two contrasted behaviors observed at laboratory scale. Thus, laboratory testing would tend to anticipate that while at rupture, the Mont Terri fault should potentially produce less induced seismicity than the LSBB fault. In addition, table 2 shows that the tendency to slip strongly differs between the three sites, with the LSBB and Tournemire faults being more prone to slip than the Mont Terri fault. This can explain in part the differences in the fault activation pressures measured at the sites. The Mont Terri fault activation required significantly higher injection pressures than the two other sites relative to their initial state-of-stress and frictional strength.

3. Hydromechanical and structural properties of fault zones in clay rich caprocks

It is difficult to relate the structure of a fault to the mechanisms of activation and leakage experienced upon pressurization because each individual fault has its own characteristics (Seebeck et al., 2016). Fault activation experiments in URLs not only provide the possibility to characterize fault zone properties in great detail, but they also allow observing how these properties change during the activation. This is key for fault zones affecting clay-rich caprocks that are difficult to observe otherwise. For example, faults outcropping at the land surface are strongly altered and experiments in deep boreholes do not allow the necessary characterization detail and monitoring resolution. In the URL studies cited in this paper, the fault zones were characterized from several fully cored boreholes (with a 80-to-100% core retrieval) drilled from nearby tunnels, from exhaustive borehole logging, and from direct observations of large fault outcrops on the gallery walls.

The architecture of fault zones is generally conceptualized as a thin fault core surrounded by a damage zone progressively transitioning into intact rock (Caine et al., 1996; Wibberley et al., 2008). The fault core is where most of the deformation is accommodated though geological time. It includes highly deformed material such as slip surfaces, shear zones, breccia, gouge, etc. The damage zone is a network of subsidiary structures, mainly fractures and secondary faults. In the fault literature, the core is often described as highly deformable and having low permeability while the damage zone is considered less deformable but highly permeable (Faulkner et al., 2010). The processes controlling hydromechanical behavior are often considered to be at granular scale in the core in contrast to fracture scale in the damage zone. Caine et al. (1996) proposed that whether a fault zone will act as a conduit, barrier, or a combined conduit-barrier system depends on the relative percentage of the fault core and damage zone structures. Using Caine's framework, it appears that the fault zones in clay-rich material tested in Mont Terri and in Tournemire display a significantly 30-to-80% smaller

damage-zone-vs-core ratio than the carbonate fault of LSBB, suggesting that strong deformation tends to be more localized in clay-rich rocks (Fig. 3). We conclude that the two faults in clay-rich rocks, representative of CO_2 storage caprock units, would tend to behave as localized barriers while the faults in carbonate reservoir would tend to function as a combined conduit-barrier system.

Another characteristic of the shale fault zones representing caprock behavior is that they contain large amounts of so-called "scaly" fabric which form an anastomosing network of polished surfaces where clay-rich rock splits into progressively smaller flakes (Vannucchi, 2020). Scaly fabric has a multi-scale structure organized into individual macroscopic lenses and is preferentially observed in phyllosilicate-rich rocks. The presence of such lenses may influence multiple modes of slip, from creep to seismic slip, and also affect the hydromechanical behavior. For example, the mesoscale fault slip experiments at Mont Terri showed significant differences in the hydromechanical response of scaly fabric lenses compared to individual fault shear planes (Guglielmi et al., 2017). Pressurization of scaly clay lenses produced complex slip on multiple planes but no significant leakage (or permeability increase) even at high pressure levels close to the fracturing pressure. In contrast, pressurization of macroscopic natural planes, such as the principal or secondary shear planes in the fault zone, consistently generated a rapid increase in leakage rate from zero to several liters per minute when the injection pressure approached the normal stress on the fault. Thus, although the permeability of inactive zones in a shale fault is as small as the permeability of the intact clay-rich rock, these zones may display a highly heterogeneous hydromechanical response to pore pressure variations depending on the presence of scaly fabric. Scaly clay lenses inside a fault core zone inhibit leakage, significantly reduce the fault zone's Young modulus by a factor of ~10 compared to the intact rock, and destroy the transverse anisotropy often related to bedding planes in the host rock (Jeanne et al., 2017).

We may contrast the shale faults at Mont Terri and Tournemire with faults situated in porous reservoir rocks, which have much lower clay content though often some clay minerals smeared in their principal shear zones (Cilona et al., 2015). While reservoir faults may also display a complex structure, they usually have an initial permeability along the fault that is significantly higher than the intact rock, specifically in the fracture damage zones surrounding the fault core. As a result, our tests conducted in the carbonate reservoir fault all showed a fundamentally different hydromechanical response to pressurization, with a much earlier progressive growth in leakage rates compared to the sudden late response in a shale fault. One reason is the strong contrast in fault architecture. Jeanne et al. (2014) showed for example that mature fault zones with a well-developed permeable damage zone can more easily evacuate overpressures. It may induce delayed and much larger seismic events, as a much larger fault zone area can be pressurized. As discussed earlier, the damage zone is generally less developed in shale faults, preventing fluids from penetrating and/or escaping from the fault zone. Another reason could be the ability of clay to deform at many different scales, thus being able to accommodate more poroelastic and plastic deformation through creep than other reservoir rock types.

4. Uncoupling between slip and permeable pathway creation in low-permeability shale faults

In Fig. 4, we compare the displacement behavior in the LSBB carbonate and the Mont Terri shale faults. Both faults were activated by water pressure step increases in borehole intervals across the vertical depth of the faults. The total injected fluid volume in the carbonate experiment was 6.6 times larger than in the shale test (950 versus 143 liters, respectively) although the duration of the carbonate experiment was only a factor of 1.7 longer than the shale test. For the same experiment duration of 850 s, injected volumes in the LSBB carbonate and in the Mont Terri shale faults respectively are of 381 and 143 liters. At 850 s, both experiments have reached the maximum injection pressure which is lower in the LSBB carbonate than in the Mont Terri shale fault, respectively, at 3.3 versus 5.4 MPa. In summary, the metrics of the two experiments are comparable, although the LSBB carbonate experiment lasted longer and injected a larger volume for a lower maximum injection pressure compared to the Mont Terri experiment.

The following main differences were observed between the

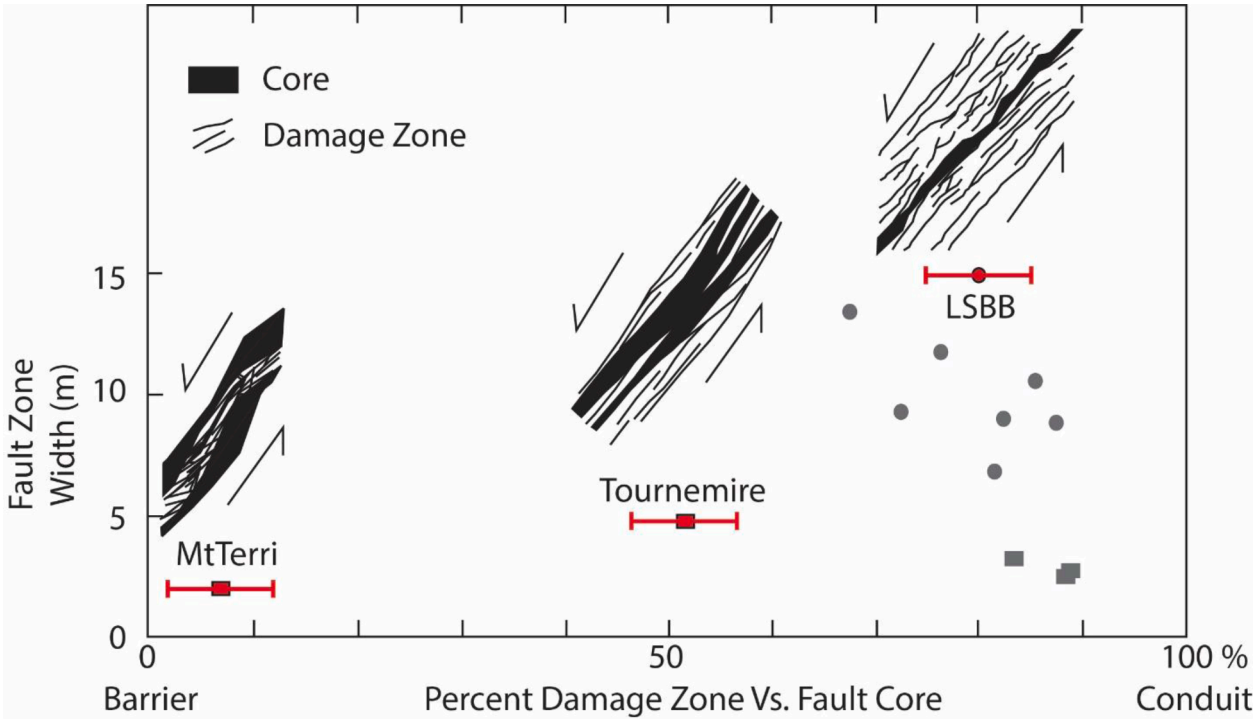

Fig. 3. Comparison of the tested faults architecture and potential permeability structure. Gray dots represent quartz-rich lithologies; gray squares represent clay-rich lithologies of fault zones studied in Caine et al. (1996).

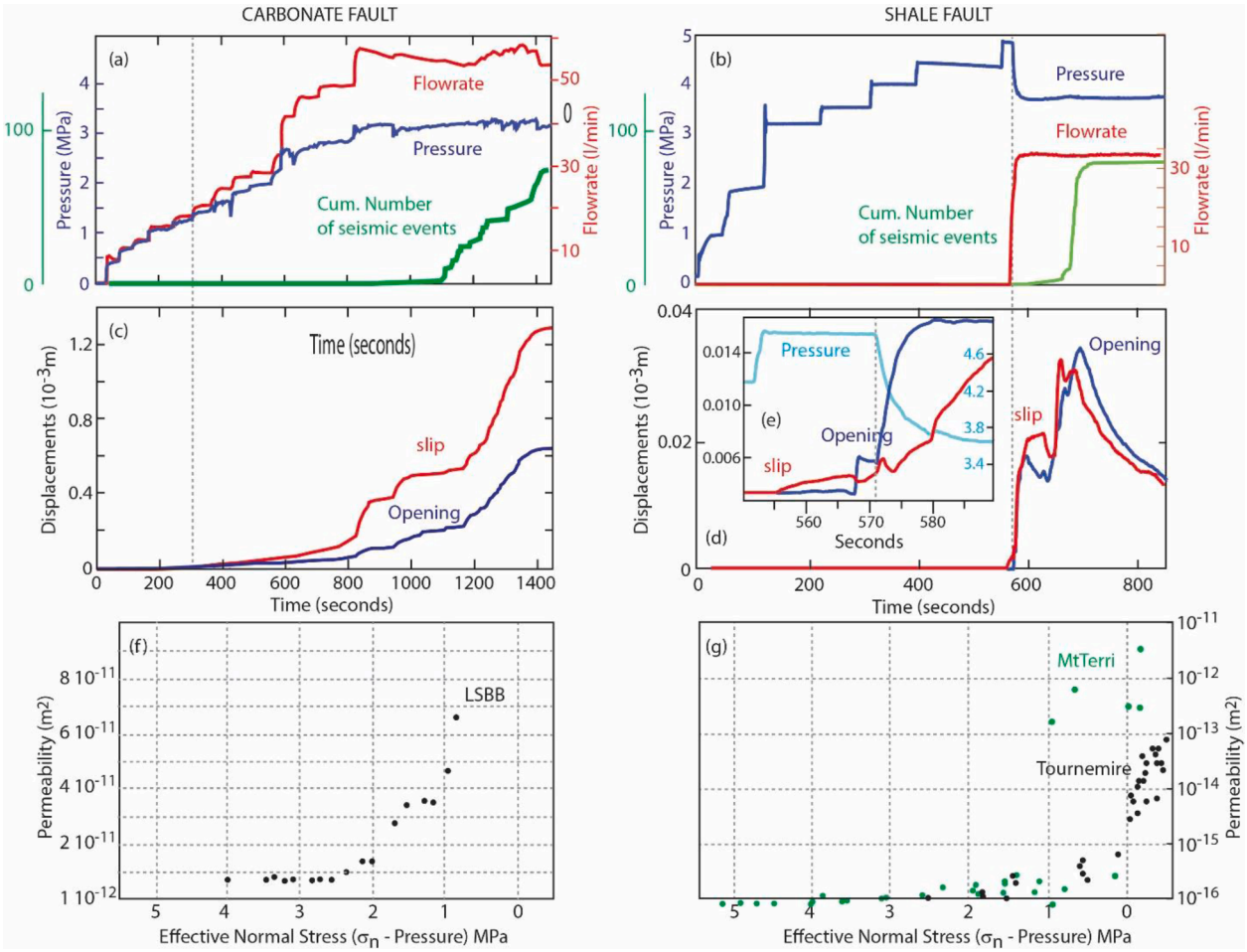

Fig. 4. Comparison of the hydromechanical response of an initial permeable reservoir fault (left column, LSBB experiment in Carbonate Reservoir) and an impermeable caprock fault (right column, Mont Terri in Shale Caprock). (a) and (b) Fault leakage response to step pressure increase; (c) and (d) Fault slip and opening; (e) Detail showing that rupture is characterized by slip preceding opening; (f) and (g) Fault permeability variation (Scale of the permeability values is different between the two graphs).

hydromechanical responses of carbonate and shale faults:

- In the carbonate fault, the injection flowrate progressively grows with injection pressure, demonstrating that the fault has initial permeability that is slowly increasing during the injection. In contrast, the shale fault remains at low permeability until a sudden flowrate increase occurs at a given threshold pressure or fault opening pressure (FOP). (Fig. 4a,b).
- Slip activation in the carbonate fault occurs at a much lower injection pressure than in the shale, although both faults display about the same normal stress values of, respectively, 4.4 and 4.9 MPa, and the carbonate fault friction is ~4 times larger than the shale fault's one (Fig. 4c,d). For activation to occur in the shale fault, the effective normal stress on the fault reduces to ~0 MPa.
- In both experiments, fault slip is associated with opening (Fig. 4c,d). However, opening of the shale fault equals or slightly exceeds the slip magnitude, while it is only half of the slip magnitude in the carbonate fault. In addition, it appears to be a slight decoupling between the timing of slip and opening events in the shale fault. Indeed, detailed observations of the fault displacements during activation identified a complex succession of such high opening events along the Mont Terri fault (Guglielmi et al., 2020a). As shown in Fig. 4e, the fault first slips then opens, highlighting that shear rupture initiates before the fluid can penetrate the fault and open it.
- The permeability of both faults increases considerably in response to fluid injection. However, the relative permeability increases are 4 to 5 times larger in the shale fault compared to the carbonate fault (Fig. 4f, g). In the shale experiments, the fault permeability displays a sharp increase when the effective normal stress applied on the fault gets close to zero. Below that value, a small but steady increase is observed similar to what is seen in the carbonate fault. This small increase may relate to dilation during slip preceding opening (Fig. 4e).

These observations were used to test different hydromechanical concepts of fault activation. Jeanne et al. (2018) showed that permeability models with a slip dependent permeability can describe the dilatant slip events observed in the shale faults. However, several parameters for the constitutive relationship describing permeability change had to be calibrated against the fault pressure measurements in order to be able to reproduce the effects of a succession of slip events. Jeanne et al. (2018) also showed that depending on the fault reactivation history, almost similar slip events can either create or destroy the fluid pathways. Thus, a succession of slip events did not typically create a continuous hydraulic pathway, which is inconsistent with the field observations in Fig. 4b, d showing a continuous flowrate (leakage pathways) associated with multiple slip events.

Other hydromechanical models were developed to investigate the sudden threshold effect observed in the permeability evolution of activated shale faults (Fig. 4g). These models typically consider a frictional stress-dependent permeability to simulate fluid flow in the activated parts in shear or tensile failure of the fault (Guglielmi et al., 2015b;

Cappa et al., 2018; Rutqvist et al., 2020; Park et al., 2020), while postulating that there is no flow occurring in the remaining elastic parts. The models were successful in reproducing the sudden and significant flow rate increases observed in the field (Fig. 4b). Simulations show that the fault is opening in the nearfield of the pressure source when the injection pressure induces a drop of the effective normal stress on the fault to almost zero. This is consistent with previous theoretical studies on clay-rich faults demonstrating that a local fluid pressure must get close to the total fault normal stress before fault slip is being triggered (Viesca and Rice, 2012). One reason for this behavior is that the faults studied in the shale experiments were not favorably "enough" oriented towards the principal stress state, "requiring" more fluid pressure to reactivate as described in previous theoretical works (Axen 1992; Rice 1992; Faulkner and Rutter, 2001; Garagash and Germanovich, 2012). Perhaps more importantly, models show that this effect is amplified by the very low initial permeability of the shale fault and by the low rigidity of the rock surrounding the fault, which together create conditions for a mixed opening and shearing rupture mode where fluids force their way through ruptured patches within the fault. As a result, the fault experiences a relatively large normal displacement measured at the injection point compared to the shear displacement.

The models discussed above are showing another important mechanism within the activated fault. Just outside of the zone of elevated fluid pressure, slip is promoted by increased shear stress rather than by the change in effective normal stress. Indeed, failure in the pressurized fault patch increases the shear stress beyond the pressure front where the shear strength reduces as a function of the slip characteristics (magnitude and velocity) (Cappa et al., 2018, 2019). Obviously, this second mechanism is intimately linked to the reduction in fault strength being more pronounced in the pressurized zone than in the immediate surrounding region. Models show that the larger the change in fault permeability in the pressurized zone, the larger is the slip zone outside of the pressurized fault patch (Cappa et al., 2018). Thus, in addition to the stress criticality of the fault, the size of the slip zone is also influenced by the size of the fault area affected by overpressure.

A mechanism of permeability increase related to slip-induced dilation represents well the hydromechanical behavior of the initially permeable carbonate fault (reservoir analog, Guglielmi et al., 2015a), while it cannot explain permeability creation in the shale fault (caprock analogue) where fluid has to force its way into and along the fault at very high pressure. Comparison of Figs. 4f and 4g highlights a more general take away about fault permeability creation during activation. In shale faults, slip is not the main process generating a significant increase in fault leakage. In contrast, slip may be the main mechanism in initially permeable faults, for example in faults with a developed fractured damage zone that may be typical of reservoir rocks. This finding is consistent with laboratory tests that show that the permeability can either enhance or reduce with slip (Rutter and Mecklenburgh, 2018; Wu et al., 2017), resulting in channeling flow or no flow, and a heterogeneous distribution of fluid pressure (Rutter and Hackston, 2017) over the stimulated feature. In shale faults, the creation of flow paths is likely more dependent on a very low effective stress environment rather than the occurrence of fault slip. We also interpret that the moderate pre-FOP permeability increase in shale faults is related to shear that occurs along these faults at much lower pressures than the normal stress value. In a way, it is similar to what is observed at the front of the pressurized zone where shear stress concentration initiates shear and an associated limited dilation that is enough to explain the slight pre-FOP permeability increase observed in Fig. 4e and 4g.

5. Dominant aseismic deformation and slow fluid leakage

The tens-of-meter scale fault reactivation experiments at Mont Terri, Tournemire and LSBB have produced low-magnitude earthquakes of roughly −4 to −2, which is partly related to the small injection volumes ranging from tens to hundreds of liters. We also observed that the experiments conducted in shale had significantly less seismic events than the experiments in reservoir (carbonate) rocks. De Barros et al. (2019) collected a detailed catalog of injection-induced seismic slip data from the LSBB and Tournemire tests that allowed for comparison between seismicity induced by fault zone activation in permeable carbonate rock and much less permeable shale. About 50 events were reported for the shale fault tests versus up-to-500 events in some of the carbonate fault tests. Core samples from both test sites were tested and pointed to differences in frictional behavior associated with differences in the fault mineralogy as the main reason the difference in observed seismicity. Indeed, in the laboratory, a velocity-strengthening regime characterizes the potentially stable frictional behavior of clay rich gouge from Mont Terri fault samples, while an increasing fraction of carbonate minerals from the LSBB site favors a velocity-weakening regime (Orellana et al., 2019). This result has led to the development of a well-established framework of frictional rate dependent behavior for clay-rich fault materials, which was shown to predict well their activation (see Bohloli et al., 2020 as a recent case study example).

Fig. 4a,b illustrate the different seismic behavior observed between the carbonate (LSBB) and the shale (Mont Terri) faults, through the plot of the cumulative number of induced seismic events versus the activation time (here we chose two stimulation experiments that roughly produced the same number of events). Interestingly, for the time period depicted, the number of events is about the same in both cases and it is relatively low. In both cases, the timing of the seismicity and the shape of the curves highlight that a significant aseismic slip occurs before seismicity. Indeed, in all of the fault reactivation experiments, we consistently observed the importance of injection-induced aseismic deformation, estimated to represent about 80-to-100% of the energy dissipated at rupture (Guglielmi et al., 2015; De Barros et al., 2019; Duboeuf et al., 2017). De Barros et al. (2019) showed that the seismic energy depends on only a fraction of the injected fluid volume (V), suggesting a $V^{3/2}$ dependency.

In the carbonate fault, the cumulative number of seismic events increases gradually with time, and seems to be closely correlated to the increase in slip, or the acceleration of slip (Fig. 4c). This suggests that seismicity is triggered by the induced slip, with shear occurring on asperities within or outside the slipping areas. In the shale experiments, seismicity is generally scarcer, and in some tests there are no observable seismic events at all. Similar to the carbonate fault, events occurred rather triggered by stress perturbation from slip rather than by the decrease in effective pressure. In Fig. 4b, the sharp increase in the number of events is due to the aftershocks of a large seismic event, i.e., these events are triggered by stress transfer from one seismic event to another. To summarize, in both cases, seismicity is chiefly triggered by stress perturbation rather than directly induced by effective stress decrease. The differences in the number of events may come from differences in (1) the amount of slip versus opening, 2) the injected volumes and therefore the size of the perturbed volume, and 3) the presence of slip/rate weakening asperities in a near critical state.

Using data from the LSBB experiment in fractured carbonates, Duboeuf et al. (2021) highlighted a significant discrepancy between stress estimated from focal mechanisms of induced seismic events and stress estimated from static fault displacements measured with the SIMFIP probe. They found that static estimation was in good accordance with the background stress, while focal mechanisms were showing a significant dispersion of both the orientation and magnitude of the stress tensor. The authors concluded that seismicity was in part reflecting local stress perturbations caused by the aseismic movements of the activated fractures. Therefore, to accurately predict the released seismic energy, aseismic deformation needs to be considered in the budget.

Our field experiments show that the physics of aseismic fault reactivation by injection of fluid are complex, and that there are multiple controlling factors, not just the mineralogy of the fault zone which is typically the dominant factor at the laboratory scale. The orientation of displacement vectors measured *in situ* show a large variability that is

related to interactions between multiple second order fractures in the fault core rather than slip on a well-defined plane (Guglielmi et al., 2020a). These displacements are associated with a wide variety of seismic vibrations, ranging from "conventional" impulsive seismic events to longer period – lower frequency events and eventually some events looking like tectonic tremors (Derode et al., 2015). To understand how aseismic fault movement can be related to seismicity, Cappa et al. (2019) conducted fully coupled hydromechanical simulations of the fault activation experiment in carbonates at LSBB (Guglielmi et al., 2015), as well as supporting laboratory-scale experiments. Their simulations confirmed that fluid pressure increase in a fault mainly induces aseismic accelerated creep, and that if seismicity occurs it is typically located just outside the pressurized fault patch where shear concentration favors unstable slip. This result is also in accordance with theoretical work that showed that high pressure in faults generates dilatancy that favors frictional rate strengthening, thus aseismicity (Segall and Rice, 1995). Localization of induced seismic events outside the pressurized patch was confirmed by the controlled field experiments in the LSBB carbonate and in the Tournemire shale where seismicity was localized with a high accuracy (Duboeuf et al., 2017; Barros et al., 2016). At Mont Terri an insufficient number of seismic sensors array did not allow accurate localization.

The different behavior of seismicity as a function of time observed in Figs. 4a,b reveals different processes not yet constrained at this point. Yet such spatio-temporal evolution of seismicity is commonly used to estimate fluid migration processes related to fluid injections and induced seismicity at the crustal scale (Shapiro et al., 2002). In such way, migration velocities of 3 to 15 m/h have been estimated for fluid injections in deep basement geothermal reservoirs (Lengline et al., 2017; Goetz-Allman et al., 2011) and to waste water injections in the deep carbonate-basement system of Oklahoma (Keranen et al., 2014). Using the seismic events recorded during the LSBB stimulations, Duboeuf et al. (2017) estimated a migration velocity in the same range of 4-to-12 m/h as these crustal scale values. However, they observed in several tests a lack of clear earthquake migration or seismicity that mainly occurred as bursts of events (Fig. 4b). This may be explained by 1) a short injection experiment duration and a small number of events and 2) the occurrence of different processes, in complex geometry settings.

Regarding fault behavior in shales, the Mont Terri activation experiment provided an opportunity to directly measure the fluid migration velocity along the hydraulic connection that formed due to rupture propagation between two vertical boreholes intersecting the fault (Fig. 5). Both boreholes, arranged at a 3 m horizontal distance, were equipped with the same downhole probe measuring the detailed evolution of pressure change and local fault displacement. Analysis of the pressure data demonstrates that the pressure pulse migrates (or fluid migration occurs) much faster than in the carbonate experiments, for a much smaller injected volume (see previous section), and also much faster than what is observed at crustal scales. We can also use displacement data from the same two boreholes to compare characteristics of fluid migration with characteristics of the propagating fault rupture. Shear displacement arrives first at the monitoring point, ~23 s after the rupture initiation at the injection source, which corresponds to a rupture velocity of ~471 m/h. Shear is associated with an increase in the total stress of ~0.5 MPa at the monitoring point. Fluid pressure arrives second, ~32 s after the rupture initiation at the injection source, which corresponds to a fluid migration velocity of ~337 m/h. The earlier arrival of the displacement front is consistent with the concept of a fluid pressure front following a rupture front in the fault, the rupture being triggered in front of the pressure front by an increase in the stress.

As also is shown in Fig. 5, a burst of seismicity is eventually recorded at the Mont Terri activation experiment, with the first event starting 83 s after the rupture initiation at the injection source, and corresponding with the onset of a large dilatant shear event recorded at the monitoring point. A seismic cluster of ~80 events started ~30 s later. Unfortunately, this experiment had only two accelerometers that could not allow precise localization of seismicity. Still, results clearly show that seismicity could not have occurred either at the injection or the monitoring points. The two seismometers were deployed at the top and bottom of the fault zone in a borehole set at a horizontal distance of 4.3 m from the injection borehole. Seismicity was mainly recorded at the top fault accelerometer. Based on amplitude, waveforms and polarization of the events, we can deduce that the seismic events must be localized in close vicinity of the top accelerometer. This is in good agreement with the concept of rupture propagating along the top of the fault away from where fluid injection takes place. Considering that at the time of the onset of seismicity, rupture must have reached the vicinity of the top accelerometer, gives a rupture velocity of ~187 m/h still much higher than observed in the

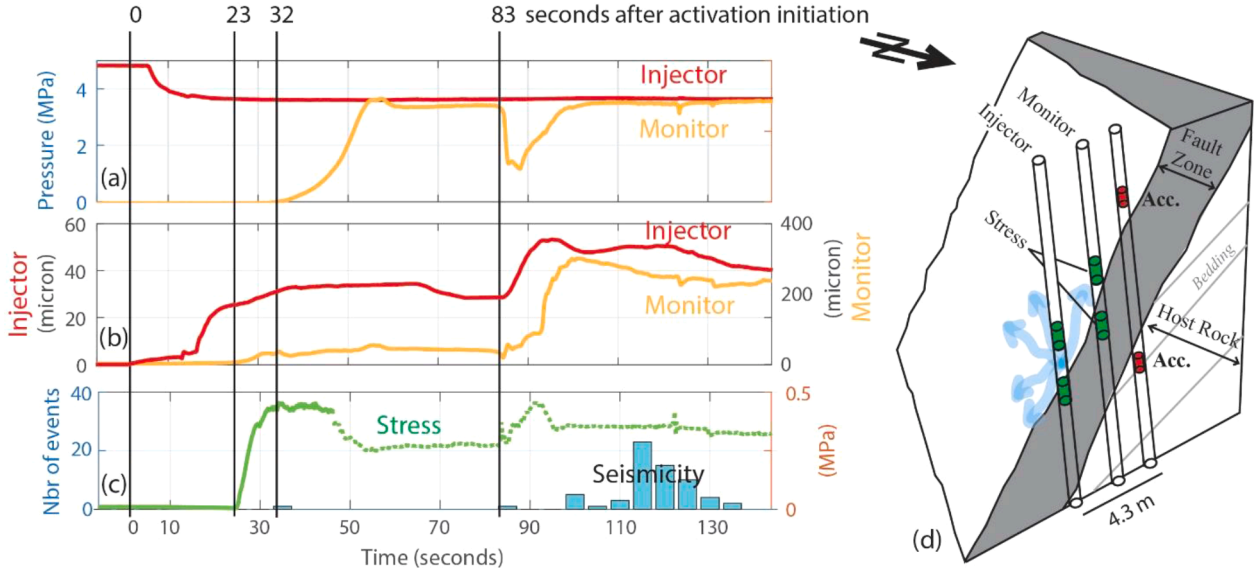

Fig. 5. Leakage migration into the Mont Terri shale fault during an experiment conducted in 2015. (a) Fault pressure at the injection and monitoring points; (b) Fault slip at the injection and the monitoring points; (c) Stress variation at the monitoring point and seismicity recorded at the two accelerometers; (d) Three-dimensional view of the fault structure and of the instrument setting (Green symbols represent the strain sensors used for stress estimation, and red symbols represent the position of accelerometers for seismic monitoring). (For interpretation of the references to color in this figure legend, the reader is referred to the web version of this article.)

LSBB experiment. In the bibliography, such fast migration velocities of the seismic front are usually related to slow-slip events (e.g. Vidale and Shearer, 2006; Lohman and McGuire, 2007) rather than to fluid diffusion.

In 2020, a similar but larger-scale experiment was conducted in a nearby location of the same Mont Terri shale fault. A similar behavior and succession of events was observed, characterized by the displacement front arriving ahead of the pressure front. The hydraulic connection along the 15 m long fault patch between monitoring boreholes was established within ~7 min, giving a fluid migration velocity of 128 m/hr. Comparison of all experiments discussed here consistently shows that fluid migration velocities in the activated shale fault are about 3 to 10 times higher than the carbonate fault, although mostly generated by aseismic fault displacement behavior.

The conceptual fault architecture models described in Fig. 3 help explain the difference in fluid migration velocities between the two types of fault rocks. In a shale fault, very little fluid migration can take place outside the ruptured area of the fault, which contrasts with the carbonate fault that has higher initial permeability. We previously explained that for leakage to occur along a shale fault, there must be fault rupture to create sufficient permeability for it to grow. We also discussed that fluids migrating in a shale fault cannot easily escape into the adjacent rock because faults in shales do not develop a large fractured damage zone and fractures in the damage zone are initially impermeable. The rupturing patch in the fault thus maintains a consistent high level of overpressure even away from the pressure source. This can be seen in Fig. 5a where the pressures at both the injection and the monitoring points "equilibrate" to almost the same values of, respectively 4.2 and 3.9 MPa after 60 s (showing almost no pressure gradient between the two points). Note the interesting pressure behavior at the monitoring point, where a large pressure drop is observed at the onset of a large slip event correlated with the onset of seismicity. We believe this pressure signal highlights the opening of a local patch of the fault which is then rapidly filled by injected fluid. No significant fluid migration seems to have been triggered beyond this limited-size patch since the pressure at the monitoring point quickly recovers to its pre-event initial value. This confirms that fluids migrating in shale faults need to force their way into ruptured zones at high pressures, which in turn favors a much faster rupture migration velocity than in permeable fault zones. Given the initially negligible fault permeability and the limited opportunity for fluids escaping into the damage zone, a stronger pressure buildup is generated despite a much more limited amount of injected fluid volume than in reservoir faults.

6. Partially irreversible post-injection fault evolution and self-sealing

To our knowledge, there are no published studies about the long-term (i.e., years after the activation event) hydromechanical behavior of a fault after a controlled field injection and fault activation experiment. We provide here insights from the October 2015 fault activation experiment at the Mont Terri URL (Fig. 6), where pore pressure monitoring was conducted for several years before and after the activation. Fig. 6a complements Fig. 4b, showing the hydromechanical response of the shale fault immediately after the activation experiment is terminated by a step decrease of the injection pressure. The following observations

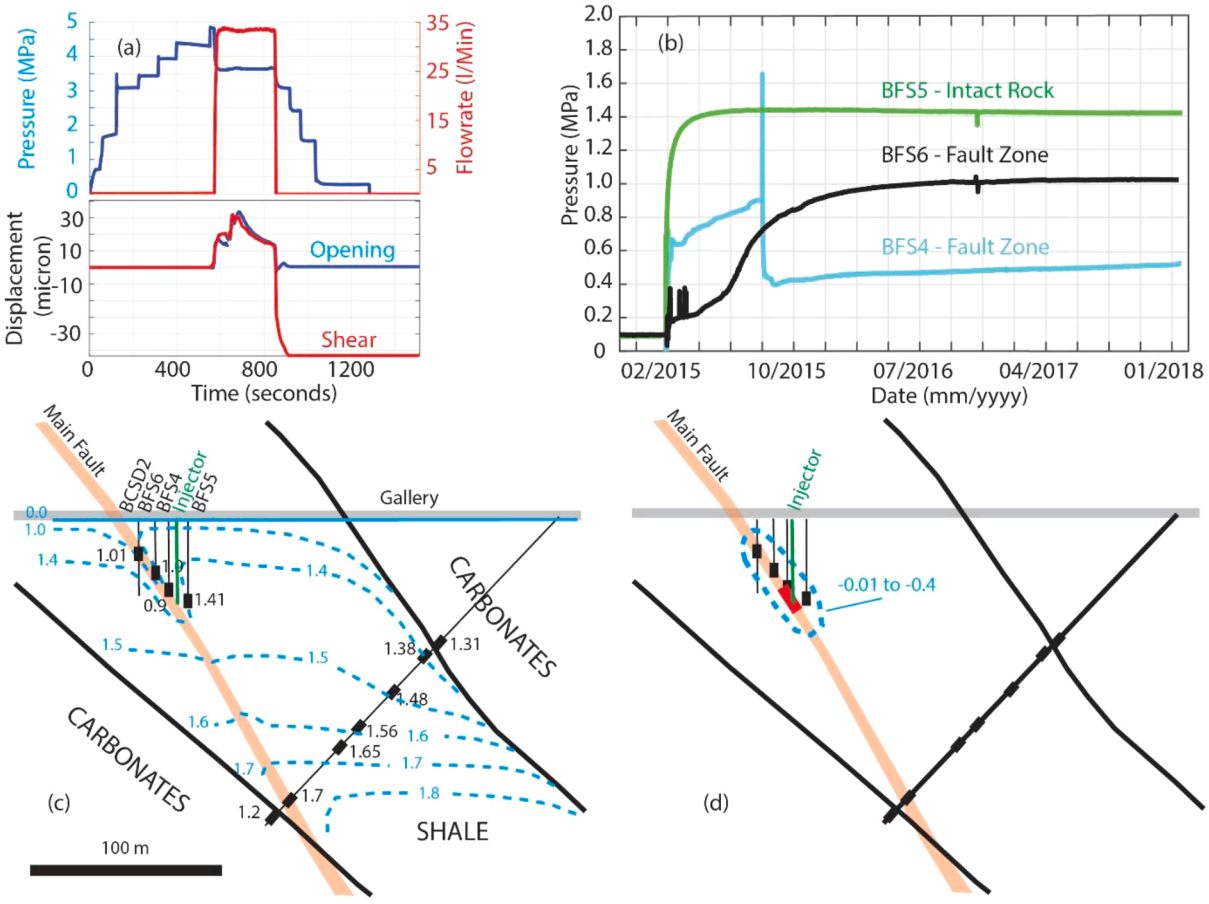

Fig. 6. Post-activation hydromechanical response of the Mont Terri shale fault. (a) Pressure, flowrate and displacement (opening, shear) measured at the injection point; (b) Long-term pore pressure response of the fault zone and of the intact rock; (c) Pore pressure (MPa) alteration of the Mont Terri shale layer by the fault zone before activation; (d) Irreversible changes in pore pressure (MPa) measured after fault activation (the fault activated segment is figured in red). (For interpretation of the references to color in this figure legend, the reader is referred to the web version of this article.)

can be made:

- As soon as pressure decreases below a pressure close to the normal stress on the fault, the flowrate falls back to zero. No back flow is measured at the injection point.
- The return of the flowrate to zero is associated with a complete closing of the fault.
- There is a significant over-shearing (shear-slip reverse back with some residual) observed at the injection point which might relate to the complex hydromechanical effects of a reversed pressure gradient (pressure at injection being smaller than away from injection) in a weakened ruptured fault patch.

Fig. 6b shows the long-term pressure response at three locations close to or within the Mont Terri fault zone (BFS4 and BFS6 respectively in Fig. 6b), and away from the fault in the intact rock (BFS5 in Fig. 6b). Monitoring started in early 2015 about 8 months before the activation experiment, and continued for 3 years after the activation experiment. Initially, the pressure values are very small due to disturbance from borehole drilling and the open URL galleries. From 02/2015 to 10/2015, the pre-activation period shows a transient pressure increase from these small values until "equilibration" with formation pressure. Compared to the two points set in the fault zone, pressure "equilibration" in the intact rock at BFS5 is much faster and gets to a steady-state higher pressure much earlier.

The BFS4 fault zone point appears to be hydraulically connected to the injection source, which explains the sharp pressure increase 2015 to 1.64 MPa observed during the short activation period in October 2015. During the month following activation, BFS4 experiences a pressure drop to 0.39 MPa, which is 0.51 MPa below the initial pore pressure. This pressure drop initiates while there is a complete mechanical closing of the fault at the injection point, when the pressure at this point is decreased to atmospheric pressure (Fig. 6a). This closing is fast. It lasts ~400 s in response to pressure decrease. The pressure drop observed at BFS4 is associated to drainage of the activated patch connecting BFS4 with the injection borehole set at atmospheric pressure. Numerical analyses of the pressure-vs-time curve give a decrease of fault permeability to a low value of $\sim 10^{-14} m^2$ that is still about two orders of magnitudes higher than the fault permeability before activation. Then, from November 2015 to the end of the monitoring period, there is a slow 0.06 MPa/yr increase in the BFS4 pressure. This long-term increase of the BFS4 pressure indicates that the permeability of the BFS4-injection borehole connection slowly decreases with time, highlighting a slow fracture sealing process.

These observations are similar to long term recovery of pore pressure disturbances observed in studies of the self-sealing of extensile fractures of the excavation damage zone (EDZ) of galleries in clay rocks (Mazurek et al., 2008). By repeating hydrotests in a Mont Terri gallery's EDZ over a 2-year time following a gallery excavation, Bossart et al. (2004) quantified a two orders of magnitude decrease of EDZ fractures permeability, respectively from 10^{-13} to 10^{-15} m^2. Bock et al. (2010) described several self-sealing mechanisms of such EDZ argillaceous extensile fractures, including fracture aperture closing under stress increase, clay mineral swelling and chemical precipitation.

At a larger scale, we have projected all the pore pressure measurements made in December 2020 across the entire Opalinus Clay layer (which is about 130 m thick), both within and away from the fault (Fig. 6c). It appears that the pore pressures are between 0.1 and 0.4 MPa smaller in the fault zone compared to the intact clay, suggesting that the fault zone is "still" draining the intact rock towards the nearest Mont Terri gallery segment which was excavated 12 years ago in 2008. This observation complements the one from the 2015–2018 continuous BFS4 pore pressure increase. First, it shows that the gallery excavation creates a fault pore pressure perturbation that extends about 50 m away within the fault zone. Second, it shows that this pressure perturbation did not recover after 12 years. The fact that the fault zone still acts as a drainage pathway either shows that there has been no complete fault sealing over time after its damage (reactivation) by gallery excavation or that the fault zone has a slightly higher permeability than the intact rock which favored the preferential drainage towards the gallery. According to Thoeny (2014), excavation of the gallery decades ago generated a lot more mechanical damage in the fault zone than in the intact rock. Using various geotechnical measurements, they estimated that the maximum extent of the EDZ was at least twice larger in the fault zone than in the intact rock, respectively >4 m and 2-to-3 m. Pressure data in Fig. 6c suggest a much larger excavation disturbed zone. In Fig. 6d, we then only plotted the irreversible pressure measured after the fault activation. We observe a permanent pressure depletion of −0.01 to −0.4 MPa recorded over a fault length of about 50–60 m (i.e., pressure did not recover to pre-stimulation value 3 years after the experiment). The permanent pressure perturbation length is thus much larger than the fault rupture patch length of ~15 m (red segment of the fault in Fig. 6d). These observations again suggest that the local fault rupture may have created slight irreversible damage in a larger volume of the fault.

On a more general point of view, the observations of pore pressures after the Mont Terri fault activation show three complementary results:

- As soon as the post activation pressure falls below approximately the fault clamping normal stress, there is an apparent mechanical closing. It has an immediate effect on stopping the large leakage flowrates measured during the high-pressure activation period.
- The hydraulic closing of the fault is not complete. There may be a small residual opening that allows for small long-term leakage. This long-term modification of the hydraulic properties of the fault could be related to the over-shearing measured at closure which may have created a network of connected micro-fractures and/or some undetectable dilation by the experiment sensors.
- Observations of long-term slow pore pressure increase in the activated fault patch may show evidence of slow sealing effects although they may not be complete. Compared to what is observed in the EDZ of originally intact clay rock, heavily faulted rocks may display such damage that sealing is much slower or remains incomplete.

7. Industrial-scale CCS projects versus fault reactivation experiments

7.1. Existing studies on reservoir pressurization, fault activation and caprock leakage for industrial-scale CCS

Taking the example of the Illinois Basin (USA), Birkholzer and Zhou (2009) showed that regional-scale pressure buildup of several MPa may occur for a hypothetical future CCS scenario with 1/3 of all large stationary emissions in the region captured and stored in the Mount Simon saline aquifer. Their simulation study assumed 20 industrial-scale projects distributed over the region, each injecting 5 million tons of CO_2 per year, over a time period of 50 years. Even though diffuse pressure bleed-off through the upper and lower sealing low-permeability layers was shown to be effective in reducing some of the pressure impacts, the modeling results nevertheless demonstrate wide-spread pressurization in the Illinois Basin with individual zones of pressure increase overlapping between neighboring projects. So what do these and other such studies as reviewed in Birkholzer et al. (2015) mean for CCS at scale and induced seismicity concerns? Let us compare the CO_2 injection volumes assumed in Birkholzer et al. (2009) with the saltwater injections into the Arbuckle basal aquifer which produced a marked and widespread increase in seismic events in Oklahoma. Starting in 2012, injection volumes increased to annual levels of more than 120 million m^3 per year (Langenbruch and Zoback, 2016), quite similar to the hypothetical CCS scenario discussed above. In other words, concerns about seismicity induced by industrial-scale CCS are real and need to be addressed, both in terms of avoiding felt or damaging earthquakes at the surface and in terms of ensuring caprock integrity. In this paper, we tackle the issue of

caprock leakage as a result of reservoir pressurization potentially leading to fault activation. We note that Birkholzer et al. (2009) found the footprint of the CO_2 plume to be much smaller than the pressure-affected region, thus one may expect situations where brine leakage can occur but not CO_2 leakage.

To date, there have been few studies assessing the potential and magnitude of CO_2 leakage as a result of large-scale reservoir pressurization causing fault activation in caprocks. Observations of natural analogs for CO_2 seepage highlight that migration along permeable faults could reach up to 1000 m/yr and could produce leakage rates of 15,000 t/yr (Jung et al., 2014; Nicol et al., 2017). These analogs provide valuable data points on the potential leakage rates facilitated by faults, but they are not necessarily representative of caprock (or shale) faults and they provide no information on the hydromechanical processes that have created the fault permeability. Most other studies on fault seal integrity and caprock leakage for industrial-scale CCS rely on coupled flow and hydromechanical modeling, often deploying idealized fault geometries and simplified fault mechanics. For example, Rutqvist et al. (2016) defined a "most unfavorable" case where CO_2 injection produces pressure buildup near an existing critically stressed fault, which intersects generic layered reservoir-caprock system with a moderate offset. Using quasi-static geomechanical modeling, they showed that the CO_2 plume can reach the fault after days/months and can sufficiently pressurize it to trigger rupture and leakage.

Above models initially considered fault permeability increase through slip induced-dilation. Using an upgraded dynamic version of the model, and considering that all the rupture was potentially seismic, Cappa and Rutqvist (2012) and later Rinaldi et al. (2014a, b) simulated induced earthquakes of up to M_w ~3 associated with creation of fault permeability and caprock leakage. Rutqvist et al. (2016) suggested that in some of their simulation scenarios even a sizable seismic event may not be capable of opening new flow paths across the entire thickness of an overlying caprock and such flow paths are very unlikely to cross a system of multiple overlying caprock units. On the other hand, the same authors caution that the seismic magnitude and potential leakage rates depend on a number of parameters and scenario assumptions, such as geologic setting, fault orientation and size, stress field, injection location relative to the fault, as well as fault and rock properties. We may add that these industrial-scale simulation results and their important findings are also highly dependent on the hydromechanical model assumptions and the constitutive relationships employed in these models that describe the complex coupling between stress, deformation, and flow in shale faults. We thus find it important to examine in Section 7.2 below how the results from our *in situ* meso-scale experiments may help improve some of the key concepts currently considered in these industrial-scale models.

7.2. Lessons learned from meso-scale experiments and implications for large-scale CCS

Here we examine the most important findings from the *in situ* fault activation experiments (as described in Section 3 through 6) and discuss what these might mean in terms of caprock integrity and fault leakage in large-scale CO_2 storage projects. We acknowledge, however, that the number of experiments analyzed in this paper is relatively limited and thus caution that more experimental work may be needed to provide a firmer basis for definitively answering all the questions posed below.

- *Has a caprock fault to be well oriented for slip in the ambient stress field to allow for enhanced fluid leakage?*

In our caprock analogue experiments, we do not observe a direct relationship between slip on the fault, hydraulic permeability increase, and induced seismicity. Three important takeaways from our controlled fault activation experiments are (1) that significant leakage rates were produced by the local activation of initially stable and seismically inactive faults, (2) that leakage in shale faults was associated to a large fault opening preceded by slip, and (3) that the experiments generated earthquakes of lower magnitudes than estimated based on the observed size of the slipping patches given the importance of aseismic fault movement. Indeed, the stimulated fault patches of ~10 to 20 m diameter should have created larger seismic events than was actually measured, which was on the order of −3.5 (De Barros et al., 2016). At crustal scale, significant fluid flow has been observed within faults of any given orientation versus ambient stress (Seebeck et al., 2014). In the context of deep crystalline basement rocks, deep borehole observations suggest that the most permeable faults and their fracture damage zones tend to have high ratios of shear to normal stress, i.e., they are most prone to slip or be critically stressed (Barton and Zoback, 1995; Townend and Zoback, 2000; Hennings et al., 2012). Multiple examples of induced seismicity in impermeable basement rocks caused by injection in overlaying permeable strata just above basement also demonstrates that the induced earthquakes occur in response to very small pressure changes on critically-stressed faults and, in most of the cases, the earthquakes occur several kilometers below the sediment/basement contact not long after injection-induced pressure changes occur, indicating these faults are permeable (Keranen et al., 2013; Goebel et al., 2016; Yeo et al., 2020). In addition, slip is expected to be slow and "aseismic" on faults that are not optimally oriented for slip, because slip cannot be faster than fluid pressure propagation which in turn depends on the change in fault permeability with slip along these faults planes as suggested by Zoback et al. (2012). In our experiments we examine this same mechanism. By increasing the pressure in the fault, controlled experiments bring the fault plane to shear instability. Nevertheless, in shale faults, the pressure increase first needs to be high enough for fault normal opening to allow for fluid penetration that can then pressurize the fault and produce shear slip. Wu et al. (2017) concluded from laboratory experiments that the complex link between slow slipping shale faults and permeability is dependent on the magnitude of the effective stress. At low effective stress, there can be dilation induced by slip while, at higher effective stress, the gouge created by fault slip tends to compact, thereby inducing an overall fault permeability decrease. We may propose that the large hydraulic opening observed in our experiments is a result of the ductile nature of shale faults where thick zones filled with soft material such as scaly clay can significantly deform before being critically stressed, favoring local stress concentrations and fluid channeling. Thus, in the context of caprock faults, the mechanisms leading to dramatic increases in permeability may be less dependent on effective stress than on the dilatant slip mechanism. In addition, leakage in caprocks appears to rely less on the frictional physics of faults than in deep crystalline basement rocks.

- *Are earthquakes a necessary prerequisite for caprock damage and fault leakage to occur?*

Earthquakes are not necessary in order for caprock damage and fault leakage to occur because slow aseismic slip and opening related to fluid pressurization may in fact generate caprock integrity and leakage issues more efficiently. If aseismic deformation indeed dominates in shale faults, then (1) monitoring of seismic signals may not provide a reliable indicator for potential caprock integrity issues, and (2) hydromechanical modeling of fault activation may miss important physics. In fact, most hydromechanical models for fault activation underestimate (or do not consider at all) the large aseismic deformations observed in our meso-scale fault activation experiments. The aseismic movements in the shale fault tests seem (1) to localize in the pressurized patch of the fault, while seismicity occurs just outside if at all (Cappa et al., 2019) and (2) to precede seismicity that may be a by-product of aseismic movement. While the magnitude of the induced micro-seismicity in our field experiments was small, this may change in industrial-scale operations as aseismic slip stresses faults below or above the injection formation. Recent studies on a hydrofracturing treatment in Canada shales show

that seismicity occurred a long time after leakage had initiated and way up-dip from the estimated pressurized area of the fault (Eyre et al., 2019). Such concept of aseismic slip in the pressurized zone that can eventually propagate beyond the pressurized zone and reach a seismogenic area was used to explain a M_w 4.1 event on January 12, 2016 that occurred ~250 m away from a hydrofracturing well set in the Duvernay shale in Canada (Eyre et al., 2019). These observations also show that seismicity may be triggered in shales due to changes in the rate and state friction parameters as also demonstrated by Kohli and Zoback (2013). Thus, both mesoscale experimental and large-scale industrial observations indicate that the direct measurement of aseismic deformation would provide useful data to complement conventional monitoring methods and new insights into the hydromechanical and seismogenic behavior of faults.

- *How can the largely aseismic deformation behavior in shale faults be explained and how can it be simulated?*

Our shale fault activation experiments show that large aseismic deformations correlate with fluid pressure variations and that they may create coexisting and co-located fault patches with undrained next to drained conditions within the activated fault zone, thus generating strong heterogeneity that limits seismicity. In reservoir rocks, drained conditions dominate, generating a more homogeneous and larger leakage pathway which is more favorable to produce seismicity. Such a difference cannot only be explained by differences in the fault mineralogy. Indeed, the large clay content of the caprock is associated with a rupture stability (rate strengthening behavior) that obviously limits the potential unstable behavior of clay-rich shale faults as has also been observed in the laboratory. The difference might be explained by the specific structure of shale fault zones containing thick lenses of scaly clay that behave as a granular high porosity, low-permeability material under shear (Goren et al., 2011). In addition, as discussed previously, shale faults have small to non-existing fracture damage zones which could allow fluids to escape from the fault. Thus, such faults reactivate only under very high pressure, a condition typically less prone to produce large seismicity (Segal and Rice, 1995). A promising proxy to better estimate caprock fault stability in the field is to assess both the amount of scaly clay as well as the ratio of core to damage zone thickness. Moreover, De Barros et al. (2019) suggested using the residual irreversible strain measured in deep boreholes (using borehole strainmeters and distributed optical fibers such as DSS or DAS for example) after fault activation as a proxy to quantify the viscoelastic volumetric strain. If strain remains hard to measure, they suggested to use proxy such as the minimal hypocentral distance from injection points and the critical fluid pressure for fault reactivation for a better prediction of the seismic moment. Finally, numerical models that (1) only allow fluid flow when fault is rupturing, (2) consider an elastic fault zone softness to represent soft lenses of scaly clay, and (3) condition the potential for induced seismicity on the volumetric strain rate may better estimate the location and magnitude of events potentially related to the loss of integrity of a cap rock. Recently, Wynants-Morel et al. (2020) used a fully coupled hydromechanical model including points (1) and (3) to demonstrate that aseismic slip dominates the slip budget, whatever the initial fault stress and the fault mineralogy, confirming some of these field observations.

- *What may the observed differences in shale versus carbonate fault behavior mean for CO_2 storage sites with a fault intersecting caprock and reservoir rocks?*

In the meso-scale field experiments, fluid was injected directly into the fault zone, which in the case of the carbonate fault caused a slow gradual pressure buildup. Mostly, this is a result of the carbonate fault having a permeable damage zone which allows the injected fluids to migrate along the fault, whereas the shale fault initially has a very low permeability until it is activated with increasing fluid pressure. The test geometry of the meso-scale experiments is of course quite different from CO_2 storage projects where injection occurs into a deep yet sufficiently permeable reservoir rock, pressure increases gradually at the injection point, and a pressurized zone grows within the reservoir as a function of time. Ultimately, this pressurized zone may encounter a fault that intersects both the reservoir and the overlying caprock. What we learned from the meso-scale experiments in carbonates is that the reservoir fault may act as mixed conduit-barrier system, which can block further migration in the reservoir and rather drive the pressure increase up and down along the fault damage zone, accompanied with dilatant slip and aseismic rupture along the fault. As shown in Fig. 7, both the pressure propagation and aseismic rupture along the reservoir fault favor fluid penetration into the overlying shale fault segment in the caprock. And as we learned from the shale fault experiments, this in turn can trigger rupture nucleation in the caprock associated with an accelerated fluid migration, which is mostly aseismic and thus hard to detect. As the aseismic rupture continues to propagate, it may encounter a seismogenic zone where it could then rapidly create a larger magnitude earthquake and a larger permeable fault patch. Fig. 7 is also highlighting that the pressurized patch in the reservoir segment of the fault is likely more distributed along the fault compared to the shale segment where a more compact patch is expected. This has a significant impact on the mode of rupture and on the faults' seismic behavior: In permeable reservoirs like limestone/granite, high-pressure fluids invade a given rock volume, which then increases the chance to encounter a critically stressed frictional fault and cause a seismic event. In a caprock setting, on the other hand, due to the low permeability of the shale fault, fluids can only migrate into the fault if some opening occurs which then may be followed by aseismic slip; there may be little impact on the neighboring shale volume and little interaction with other faults in the vicinity.

Will rupture expand and fluids penetrate all the way through the caprock into an overlying reservoir? Or will the sudden opening of a larger fault patch cause a significant pressure decrease (as seen in the shale fault experiment), which could close the caprock fault segment and arrest further slip? And how will such a system evolve as time progresses, as the underlying CO_2 storage reservoir will continue to repressurize the reservoir fault, at least as long as injection continues. Can such faults create a hydromechanically unstable pulsing system with sudden pressure drops and followed by pressure increases? These are key questions which we will only be able to answer with a combination of full-scale experiment and improved simulation models for reservoir-caprock fault systems (see more below).

- *Is the shale fault hydromechanical behavior inferred from hour-long controlled pressurizations experiments valid when considering 10 to 100 years pressurization?*

The answer is potentially yes because the leakage of the fault activated under pressure may be a relatively fast process. Our short-term experiments show that the propagation velocity of a permeable slip patch in a shale fault is fast, in the range of 100 to 200 m/hr. These results suggest that a CO_2 brine or CO_2 gas leak may trigger local opening of the fault zone and enable upward-migration within a discrete flow path. Nevertheless, it is difficult to estimate from short-term and limited-volume injection experiments how localized and how long the leakage pathway will remain over a 10 to 100 years pressurization. In an attempt to find natural analogs, there is a large set of basin-scale seismic observations of focused fluid escape flowpaths of meters to hundreds of meters diameter (called fluid escape pipes or chimneys) in low permeability caprocks (Cartwright and Santamarina, 2015). Some of these pipes are aligned, suggesting they may follow faults or structural heights (Loseth et al., 2011). Mechanisms such as hydrofracturing, viscous creep and decompaction weakening of the rock matrix are invoked to describe their mode of formation (Räss et al., 2018). In our shale fault experiments, we observe "similar" mechanisms of transient permeability increase related to complex fault rupture, such as a strong decrease of

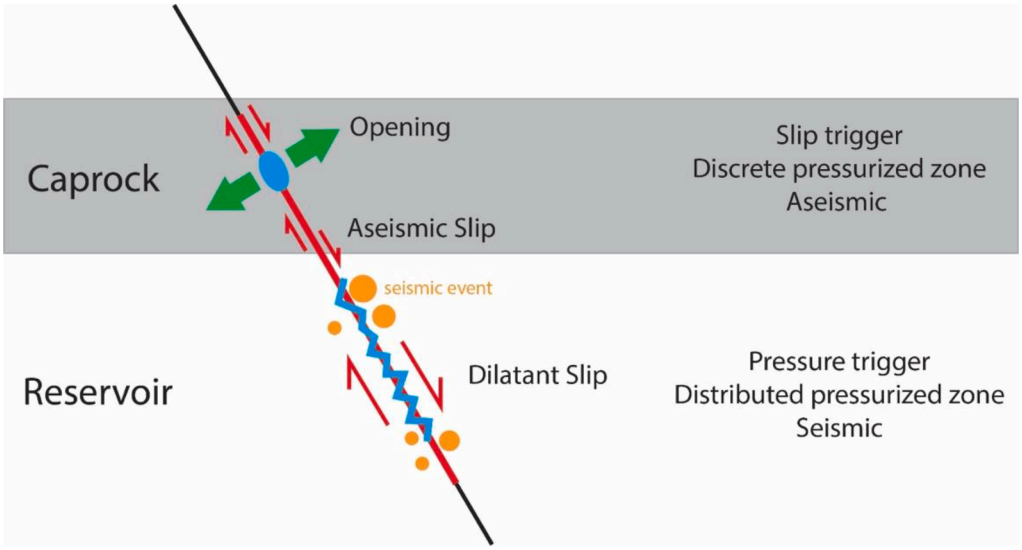

Fig. 7. Comparison of fault activation mechanisms in a conceptual reservoir-caprock system.

normal stress, slip and large dilation. Recent modeling calculated that vertical fluid migration rates in these fluid escape pipes are in the same range in both initially impermeable shale (10^{-19} m^2) and in initially permeable sandstones (10^{-15} m^2) (Räss et al., 2018). This is similar to our observations in the short-term experiments which suggest that the permeability of shale faults can be in the range of reservoir faults once they have hydromechanically opened (Fig. 4e-f). If shale fault permeability develops in such focused channels, it may have some consequences on induced seismicity. Indeed, the probability of a large magnitude event may not increase with the injected fluid volume since the fluid may not spread as far into the shale fault zones compared to reservoir faults as discussed before. In addition, the upward-migration of the highly permeable flowpath within the fault may trigger active fluid drainage from the immediate surrounding regions within the fault zone, leading to localized compaction and seismic stability. After the breakthrough, observations of 1 km long fluid escape pipes in shales overlying a source reservoir show that it may "only" take hours to weeks before the pore pressure in the reservoir drops and the blow-out terminates (Loseth et al., 2011).

- *Can shale fault rupture lead to long-term caprock integrity and leakage issues after pressure conditions have returned to "normal" (i.e., below activation pressure)?*

The answer is potentially yes although there is a lack of data about the long-term behavior of shale faults that have been activated and ruptured. Our experiments show an apparent mechanical closure as soon as fluid pressure in the fault is decreased, corresponding to an increase in the effective normal stress applied on the fault. This closing almost immediately stops the large leakage event. Nevertheless, a residual fault permeability remains which in our experiments is a few orders of magnitude higher than the fault permeability before activation. This residual permeability tends to decrease over several years following activation, highlighting some slow-acting sealing mechanism. The residual permeability might be due to damage-induced porosity related to the significant shear component affecting the fault zone during and after reactivation. This dual short term pressure-dependent closure and long term slow-acting fault self-sealing behavior might relate to the complex fault zone architecture which contains low indurated scaly clay lenses intercalated with moderate-to-high indurated fractured lenses. Indeed, it is recognized that the self-sealing depends on the type of clay minerals, the degree of induration and the chemistry of the fluid (Bock et al., 2010). Bourg (2015) highlighted a correlation between the clay mineral mass fraction X_{clay} and the unconfined compressive strength from a compilation of laboratory experimental data of shales and mudstone rocks. A sharp threshold at $X_{clay} \sim 1/3$ separates sealing shales from brittle shales. Looking at EDZ evolution in clay galleries and at natural analogues, Bock et al. (2010) estimate that low indurated argillaceous rocks self-seal in a few months while it takes several years for highly indurated (i.e., highly brittle) argillaceous rocks to seal. Rybacki et al. (2016) made similar observations on the evolution of hydraulic fractures in deep oil and gas boreholes, suggesting that shales with high brittleness tend to slowly close hydraulically created fractures. Again, in a shale fault zone, the potential for self-sealing might depend on the ratio between low and high indurated materials, and we suggest that it might depend on the percentage of scaly clay in the fault zone.

7.3. Recommended future research

The meso-scale fault experiments evaluated in this paper have provided a number of new findings with important implications for the seal integrity of CO_2 storage formations. We learned that (1) significant leakage can occur along an initially impermeable fault despite "limited" fault activation, (2) aseismic fault movement dominates the energy budget as a result of volumetric strain only partly linked to fault slip, and (3) post-activation sealing of the fault may be limited due to irreversible damage. Important research challenges remain, both in terms of understanding the complex physics of shale fault activation as explored in the experiments and in terms of translating results from these experiments into an ability to assess, monitor and predict the behavior of faulted caprocks overlying large-scale CO_2 storage reservoirs. In addition to the size and duration of injection-induced pressure increases as well as the geometry of the faults and their location relative to the injection location, we may also expect the geochemistry of the fault activation fluids to be different between our experiments (pure water) and actual CO_2 sequestration conditions (potentially CO_2-brine mixtures). Accordingly, our recommendations for future research fall into three main categories: (1) to further advance the scientific underpinnings of fault activation in caprocks, (2) to improve monitoring techniques for shale faults at different scales, specifically tools that can detect precursors for aseismic movements and caprock leakage, and (3) to develop reliable and validated models for predicting caprock integrity in field-scale projects. Given the valuable findings from the past experiments, we propose here to make advancements in all three categories by developing test-beds for the research of shale fault activation in CO_2 sequestration, at two relevant scales:

- *Meso-scale*

Additional meso-scale experiments with similar design appear crucial to augment the repeatability and the generalization of the results presented in this paper. It is first crucial to acknowledge that there is a large variety of argillaceous rocks. The experiments presented here were conducted in the Opalinus clay of Mont Terri, and in the Toarcian clay of Tournemire, which are considered moderately indurated clay rocks. Developing experiments in low indurated rocks and in high indurated rocks would be interesting to better estimate how fault structure, local stress conditions, rupture propagation modes, coupling with permeability and self-sealing vary with the argillaceous rock brittleness. Second, there is crucial lack of long-term experiments, i.e., experiments that span over several years. Such long-term experiments can only be conducted in the quiet and highly controlled environments of underground research laboratories, away from any industrial project. The long-term pressurization of a fault zone is technically difficult to achieve because it involves injecting a large volume of fluid in the fault, and thus it will expand the stimulated volume way beyond the controlled experiment volume. Exploring the long-term post-pressurization processes is a much more realistic goal. It would allow making progress in the knowledge of fault self-sealing and creep processes. Finally, improved and additional monitoring can answer remaining questions that arose from the fault activation experiments discussed above. Such experiments would utilize advanced high-resolution techniques for time-lapse imaging of fault rupture and leakage to be able to track in great spatiotemporal detail the propagating rupture and pressurized patches and their heterogeneities. Injections could be done with pure water but also with CO_2-brine mixtures to investigate whether geochemical interactions between the injected fluids and the fault rock might change its frictional seismic stability. The tests would improve our basic understanding of fault behavior; they would also provide extremely useful data to challenge hydromechanical models and improve model predictions. Advances have already been made in this area. In 2019, two new experiments called CS-D and FS-B were installed in the same fault intersecting the Mont Terri underground research laboratory in Switzerland. The ongoing experimental campaign envisions multiple injection tests (including with CO_2-brine mixtures) over the next few years and comprises new types of measurements to track the long-term leakage in the fault, including (1) tracing of water geochemistry, (2) distributed strain monitoring using optical fibers for acoustic signals, temperature and strain, and (3) time-lapse active seismic imaging across the fault zone using boreholes that straddle the fault from above and below. We expect to learn much more about how high-pressure fluids force their way along the fault zone, whether leakage occurs in a channelized and heterogeneous manner, and if the spatiotemporal characteristics of evolving leakage patterns are correlated (or not) with fault movements.

- *Field-scale*

Ultimately, it will be necessary to develop one or more full-scale testbeds for fault activation in reservoir-caprock systems affected by pressure buildup from geological CO_2 sequestration at scale, to ensure that the full geologic complexity of CO_2 storage is represented and that the behavior inferred from our meso-scale experiments remains valid when considering larger-scale decadal pressurization. We argue that this can be achieved by strategically adding government-sponsored research components to future industrial-scale CO_2 storage projects where moderate-size faults are known to exist at some distance from the injection location. Targeting fault behavior and caprock integrity, these testbeds would involve dedicated monitoring boreholes drilled into a selected fault that is projected to experience pressure impacts from injection. Similar to the meso-scale experiments but at larger scale and cost, such monitoring would allow for initial fault characterization followed by continuous measurements of long-term fault pressurization, movement, leakage and induced seismicity, as the CO_2 reservoir slowly pressurizes. Results from these experiments, obtained at the spatial and temporal scales employed in commercial CCS projects, would feed into improved hydromechanical models for the prediction and risk assessment of caprock integrity issues in reservoir-caprock systems. Such testbeds would also be useful for testing of new strategies for the mitigation and management of pressure buildup and fault reactivation concerns.

8. Summary and conclusions

The meso-scale field scale experiments analyzed in this study are bridging laboratory-scale investigations and industrial-scales field projects. They allow very detailed ~10-m scale phenomenological observations on rupture nucleation, propagation and associated fluid leakage in a shale fault zone subject to fluid injection. Key findings are that large leakage flow rates have been measured although fault activation was limited in time and in injected fluid volume, that the fault rupture was largely aseismic, and that after activation the fault clamped to almost zero permeability, although not a complete seal. These results help refine some of the claims made in Zoback and Gorelick (2012) that, given the critically stressed nature of the crust, there is a high probability that the consequent pressure elevation in the injected reservoir triggers earthquakes which may in turn damage the caprock and ruin the objective of keeping CO_2 stored deep underground. They also add perspective to Vilarrasa et al. (2015) who counter their claim with the argument (among others) that induced earthquakes due to geologic CO_2 storage are unlikely because sedimentary formations, which are softer than the crystalline basement, are rarely critically stressed. First, our field experiments show that shale faults, if they rupture, allow for significant leakage as a result of local activation. However, we also demonstrate that the earthquakes triggered by shale fault activation might be of lower magnitude then estimated based on rupture size given the importance of aseismic fault movement. The fact that aseismic movement dominates fault activation suggests that measurements of seismicity can hardly be used to track loss of caprock integrity, but that new monitoring approaches to detect aseismic deformations would be very useful. Finally, we propose based on meso-scale observations that fault leakage in low permeable caprocks may suddenly stop if the fluid pressure decreases as a result of the rapid opening of a larger fault patch. Yet this phenomenon may be short-lived in shale faults that are connected to a deeper CO_2 storage reservoir which experiences large-scale and long-term pressurization.

Declaration of Competing Interest

The authors declare that they have no known competing financial interests or personal relationships that could have appeared to influence the work reported in this paper.

Acknowledgments

Funding for Berkeley Lab's review of the field scale experiments results described in this study was provided by the Assistant Secretary for Fossil Energy as part of the Core Carbon Storage and Monitoring Research (CCSMR) and National Risk Assessment Partnership (NRAP) programs of the U.S. Department of Energy under contract DEAC02–05CH11231.

References

Amann, F., Gischig, V., Evans, K., Doetsch, J., Jalali, R., Valley, B., Krietsch, H., Dutler, N., Villiger, L., Brixel, B., Klepikova, M., Kittila, A., Madonna, C., Wiemer, S., O.Saar, M., Loew, S., Driesner, T., Maurer, H., Giardini, D, 2018. The seismo-hydromechanical behavior during deep geothermal reservoir stimulations: open questions tackled in a decameter-scale in situ stimulation experiment. Solid Earth 9 (1), 115–137.

Axen, G.J., 1992. Pore pressure, stress increase, and fault weakening in low-angle normal faulting. J. Geophys. Res. 97, 8979–8991 (doi:10.1029/92JB00517) 35.
Bardainne, T., Dubos-Sallée, N., Sénéchal, G., Gaillot, P., Perroud, H., 2008. Analysis of the induced seismicity of the Lacq gas field (Southwestern France) and model of deformation. Geophys. J. Int. 172 (3), 1151–1162.
Birkholzer, J.T., Zhou, Q., 2009. Basin-scale hydrogeologic impacts of CO_2 storage: capacity and regulatory implications. Int. J. Greenh. Gas Control 3 (6), 745–756.
Birkholzer, J.T., Oldenburg, C.O., Zhou, Q., 2015. CO2 migration and pressure evolution in deep saline aquifers. Special issue on state of the art –10 Years on from IPCC/SRCCS. Int. J. Greenh. Gas Control 40, 203–220.
Bohloli, B., Soldal, M., Smith, H., Skurtveit, E., Choi, J.-.C., Sauvin, G., 2020. Frictional properties and seismogenic potential of caprock shales. Energies 2020 (13), 6275. https://doi.org/10.3390/en13236275.
Bock, H., Dehandschutter, B., Martin, C.D., Mazurek, M., Haller, A., Skoczylas, F., Davy, C.A., 2010. Self-sealing of Fractures in Argillaceous Formations in the Context of Geological Disposal of Radioactive Waste. Report to the Nuclear Energy Agency. ISBN: 978-92-64-99095-1. https://www.oecd-nea.org/jcms/pl_14208/self-sealing-of-fractures-in-argillaceous-formations-in-the-context-of-geological-disposal-of-radioactive-waste?details=true.
Bossart, P., Trick, T., Meier, P.M., Mayor, J.C., 2004. Structural and hydrogeological characterisation of the excavation-disturbed zone in the Opalinus Clay (Mont Terri Project, Switzerland). Appl. Clay. Sci. 26, 429–448.
Bourg, I.C., 2015. Sealing shales versus brittle shales: a sharp threshold in the material properties and energy technology uses of fine-grained sedimentary rocks. Environ. Sci. Technol. Lett. 2, 255–259, 2015.
Caine, J.S., Evans, J.P., Forster, C.B., 1996. Fault zone architecture and permeability structure. Geology 24 (11), 1025–1028. November 19963 figures; 1 table.
Cappa, F., Scuderi, M.M., Collettini, C., Guglielmi, Y., Avouac, J.P., 2019. Stabilization of fault slip by fluid injection in the laboratory and in situ. Sci. Adv. EAAU4065, 13 Mar. 2019.
Cappa, F., Guglielmi, Y., Nussbaum, C., Birkholzer, J., 2018. On the relationship between fault permeability increases, induced stress perturbation, and the growth of aseismic slip during fluid injection. Geophys. Res. Lett. 45 (20), 28 October 2018Pages 11,012-11,020.
Cappa, F., Rutqvist, J., 2012. Seismic rupture and ground accelerations induced by CO2 injection in the shallow crust. Geophys. J. Int. 190 (3), 1784–1789, 2012.
Cartwright, J., Santamarina, C., 2015. Seismic characteristics of fluid escape pipes in sedimentary basins: implications for pipe genesis. Mar. Pet. Geol. 65, 126–140.
Cilona, A., Aydin, A., Johnson, N.M., 2015. Permeability of a fault zone crosscutting a sequence of sandstones and shales and its influence on hydraulic head distribution in the Chatsworth Formation, California, USA. Hydrogeol. J. 23, 405–419. DOI 10.1007/s10040-014-1206-1.
Collettini, C., Di Stefano, G., Carpenter, B.M., Scarlato, P., Tesei, T., Mollo, S., Chiaraluce, L., 2014. A novel and versatile apparatus for brittle rock deformation. Int. J. Rock Mech. Min. Sci. 66, 114–123. https://doi.org/10.1016/j.ijrmms.2013.12.005.
Cornet, F.H., 2000. Rapport du Laboratoire de Mécanique des Roches. Département de Sismologie, Institut de Physique du Globe de Paris. Rapport N°98N33/0073.
Cuss, R.J., Harrington, J.F., Noy, D.J., Sathar, S., Norris, S., 2015. An experimental study of the flow of gas along synthetic faults of varying orientation to the stress field: implications for performance assessment of radioactive waste disposal. J. Geophys. Res. Solid Earth 120, 3932–3945. https://doi.org/10.1002/2014JB011333.
Cuss, R.J., Harrington, J.F., 2016. An experimental study of the potential for fault reactivation during changes in gas and pore-water pressure. Int. J. Greenh. Gas Control 53, 41–55.
De Barros, L., Cappa, F., Guglielmi, Y., Duboeuf, L., Grasso, J.L., 2019. Energy of injection-induced seismicity predicted from in-situ experiments. Nat., Sci. Rep. 9 (2019). Article number: 4999.
De Barros, L., Daniel, G., Guglielmi, Y., Rivet, D., Caron, H., Payre, X., Bergery, G., Henry, P., Castilla, R., Dick, P., Barbieri, E., Gourlay, M., 2016. Fault structure, stress or pressure control of the seismicity in shale? Insights from a controlled experiment of fluid-induced fault reactivation. J. Geophys. Res. DOI 10.1002/2015JB012633.
Derode, B., Guglielmi, Y., De Barros, L., Cappa, F., 2015. Seismic responses to fluid pressure perturbations in a slipping fault. Geophys. Res. Lett. 42 https://doi.org/10.1002/2015GL063671.
Dieterich, J.H., 1979. Modeling of rock friction - 1. Experimental results and constitutive equations. J. Geophys.Res. 84, 2161–2168.
Dieterich, J.H., Carter, N.L., Friedman, M., Logan, J.M., 1981. Constitutive properties of faults with simulated gouge. In: Stearns, D.W. (Ed.), Mechanical Behavior of Crustal Rocks., Geophysical Monograph Series, vol.24. American Geophysical Union, Washington, DC, pp. 103–120.
Duboeuf, L., De Barros, L., Kakurina, M., Guglielmi, Y., Cappa, F., Valley, B., 2021. Aseismic deformations perturb the stress state and trigger induced seismicity during injection experiments. Geophys. J. Int. 224 (2021), 1464–1475.
Duboeuf, L., De Barros, L., Cappa, F., Guglielmi, Y., Deschamps, A., Seguy, S., 2017. Aseismic motions drive a sparse seismicity during fluid injections into a fractured zone in a carbonate reservoir. J. Geophys. Res. 122, 8285–8304. https://doi.org/10.1002/2017JB014535.
Eyre, T., Eaton, D.W., Garagash, D., Zecevic, M., Venieri, M., Weir, R., Lawton, D.C., 2019. The role of aseismic slip in hydraulic fracturing–induced seismicity. Sci. Adv. 5 (8) https://doi.org/10.1126/sciadv.aav7172, 28 Aug 2019eaav7172.
Fang, Y., Elsworth, D., Wang, C., Jia, Y., 2018. Mineralogical controls on frictional strength, stability, and shear permeability evolution of fractures. J. Geophys. Res. 123, 3549–3563. https://doi.org/10.1029/2017JB015338.
Faulkner, D.R., Jackson, C.A.L., Lunn, R.J., Schlische, R.W., Shipton, Z.K., Wibberley, C. A.J., Withjack, M.O., 2010. A review of recent developments concerning the structure, mechanics and fluid flow properties of fault zones. J. Struct. Geol. 32 (11), 1557–1575. https://doi.org/10.1016/j.jsg.2010.06.009, 2010ISSN 0191-8141.
Faulkner, D.R., Rutter, E.H., 2001. Can the maintenance of overpressured fluids in large strike-slip fault zones explain their apparent weakness? Geology 29, 503–506 doi: 10.1130/0091-7613(2001)029<0503:CTMOOF>2.0.CO;2.
Garagash, D.I., Germanovich, L.N., 2012. Nucleation and arrest of dynamic slip on a pressurized fault. J. Geophys. Res. 117, B10310. https://doi.org/10.1029/2012JB009209.
Global CCS Institute (2020). Global Status of CCS 2020. Melbourne, Australia.
Goertz-Allmann, B.P., Goertz, A., Wiemer, S., 2011. Stress drop variations of induced earthquakes at the Basel geothermal site. Geophys. Res. Lett. 38 https://doi.org/10.1029/2011GL047498 n/a-n/a.
Goren, L., Aharonov, E., Sparks, D., Toussaint, R., 2011. The mechanical coupling of fluid-filled granular material under shear. Pure Appl. Geophys. 168 (12), 2289–2323.
Guglielmi, Y., Cappa, F., Lanc, H., Janowczyk, J.B., Rutqvist, J., Tsang, C.-F., Wang, J.S. Y., 2014. ISRM suggested method for step-rate injection method for fracture in-situ properties (SIMFIP): using a 3-component Borehole Deformation Sensor. Rock Mech. Rock Eng. 47, 303–311.
Guglielmi, Y., Cappa, F., Avouac, J.P., Henry, P., Elsworth, D., 2015a. Seismicity triggered by fluid-injection-induced aseismic slip. Science 348, 1224. https://doi.org/10.1126/science.aab0476.
Guglielmi, Y., Elsworth, D., Cappa, F., Henry, P., Gout, C., Dick, P., Durand, J., 2015b. In situ observations on the coupling between hydraulic diffusivity and displacements during fault reactivation in shales. J. Geophys. Res. Solid Earth 120, 7729–7748. https://doi.org/10.1002/2015JB012158.
Guglielmi, Y., Birkholzer, J., Rutqvist, J., Jeanne, P., Nussbaum, C., 2017. Can fault leakage occur before or without reactivation? results from an in situ fault reactivation experiment at mont terri. 13th international conference on greenhouse gas control technologies, GHGT-13, 14-18 November 2016, Lausanne, Switzerland. Energy Proc. 114 (2017), 3167–3174.
Guglielmi, Y., Nussbaum, C., Jeanne, P., Rutqvist, J., Cappa, F., Birkholzer, J., 2020a. Complexity of fault rupture and fluid leakage in shale: insights from a controlled fault activation experiment. J. Geophys. Res. 125 https://doi.org/10.1029/2019JB017781 e2019JB017781.
Guglielmi, Y., Nussbaum, C., Rutqvist, J., Cappa, F., Jeanne, P., Birkholzer, J., 2020b. Estimating perturbed stress from 3-D borehole displacements induced by fluid injection in fractured or faulted shales. Geophys. J. Int. 221 (2020), 1684–1695. https://doi.org/10.1093/gji/ggaa103.
Hennings, P., Allwardt, P., Paul, P., Zahm, C., Reid Jr., R., Alley, H., Kirschner, R., Lee, B., Hough, H., 2012. Relationship between fractures, fault zones, stress, and reservoir productivity in the Suban gas field, Sumatra, Indonesia. Am. Assoc. Pet. Geol. Bull. 96 (4), 753–772 (April 2012).
IPCC (2018) Global warming of 1.5 °C. An IPCC Special Report on the impacts of global warming of 1.5 °C above pre-industrial levels and related global greenhouse gas emission pathways, in the context of strengthening the global response to the threat of climate change.
Jeanne, P., Guglielmi, Y., Cappa, F., Rinaldi, A., Rutqvist, J., 2014. Effects of lateral permeability evolution on faults zones reactivation by industrial fluid pressurization in deep reservoir: application to CO2 sequestration problems. J. Struct. Geol. 62, 97–108. May 2014 pages.
Jeanne, P., Guglielmi, Y., Rutqvist, J., Nussbaum, C., Birkholzer, J., 2018. Permeability variations associated with fault reactivation in a claystone formation investigated by field experiments and numerical simulations. J. Geophys. Res. 123, 1694–1710. https://doi.org/10.1002/2017JB015149.
Jeanne, P., Guglielmi, Y., Cappa, F., 2012. Multiscale seismic signature of a small fault zone in a carbonate reservoir: relationships between VP imaging, fault zone architecture and Cohesion. Tectonophysics 554-557, 185–201.
Jeanne, P., Guglielmi, Y., Rutqvist, J., Nussbaum, C., Birkholzer, J., 2017. Field characterization of elastic properties across a fault zone reactivated by fluid injection. J. Geophys. Res. Solid Earth 122, 6583–6598. https://doi.org/10.1002/2017JB014384.
Jung, N.H., Han, W.S., Watson, Z.T., Graham, J.P., Kim, K.Y., 2014. Fault-controlled CO2 leakage from natural reservoirs in the Colorado Plateau, East Central Utah. Earth Planet. Sci. Lett. 2014 (403), 358–367.
Kaven, J.O., Hickman, S.H., McGarr, A.F., Ellsworth, W.L., 2015. Surface monitoring of microseismicity at the Decatur, Illinois, CO2 Sequestration Demonstration Site. Seismol. Res. Lett. 86, 1096–1101.
Keranen, K.M., Savage, H.M., Abers, G.A., Cochran, E.S., 2013. Potentially induced earthquakes in Oklahoma, USA: links between wastewater injection and the 2011 Mw 5.7 earthquake sequence. Geology 41, 699–702.
Keranen, K.M., Weingarten, M., Abers, G.A., Bekins, B.A., Ge, S., 2014. Sharp increase in central Oklahoma seismicity since 2008 induced by massive wastewater injection. Science 345, 448–451. https://doi.org/10.1126/science.1255802.
Keranen, K.M., Weingarten, M., 2018. Induced Seismicity. Annu. Rev. Earth Planet. Sci. 2018 (46), 149–174.
Kohli, A.H., Zoback, M.D., 2013. Frictional properties of shale reservoir rocks. J. Geophys. Res. Solid Earth 118, 5109–5125. https://doi.org/10.1002/jgrb.50346.
Lefèvre, M., Guglielmi, Y., Henry, P., Dick, P., Gout, C., 2016. Calcite veins as an indicator of fracture dilatancy and connectivity during strike-slip faulting in Toarcian shale (Tournemire tunnel, Southern France). J. Struct. Geol. 83, 73–84. February 2016.
Lengliné, O., Boubacar, M., Schmittbuhl, J., 2017. Seismicity related to the hydraulic stimulation of GRT1, Rittershoffen, France. Geophys. J. Int. https://doi.org/10.1093/gji/ggw490 ggw490.

Lohman, R.B., McGuire, J.J., 2007. Earthquake swarms driven by aseismic creep in the Salton Trough, California. J. Geophys. Res. 112, B04405. https://doi.org/10.1029/2006JB004596.
Løseth, H., Wensaas, L., Arntsen, B., Hanken, N.M., Basire, C., Graue, K., 2011. 1000 m long gas blow-out pipes. Marine Pet. Geol. 28, 1047–1060.
Mazurek, M., Gautschi, A., Marschall, P., Vigneron, G., Lebon, P., Delay, J., 2008. Transferability of geoscientific information from various sources (study sites, underground rock laboratories, natural analogues) to support safety cases for radioactive waste repositories in argillaceous formations. Phys. Chem. Earth 33, S95–S105.
McGarr, A., 2014. Maximum magnitude earthquakes induced by fluid injection. J. Geophys. Res. Solid Earth 119, 1008–1019. https://doi.org/10.1002/2013JB010597.
Michael, K., Avijegon, A., Ricard, L., Strand, J., Freifeld, B., Woitt, M., Pervukhina, M., Tertyshnikov, K., Pevzner, R., Rachakonda, P., Larcher, A., Dance, T., Myers, M., Delle-Piane, C., Feitz, A., Stalker, L., Myers, J., Langhi, L., Hortle, A, 2019. The CSIRO in-situ laboratory – a facility For CO2 injection testing and monitoring in a fault zone. In: ECCSEL Workshop Underground laboratories for CO2 geological storage research, 5-6 June 2019. Nancy, France, p. 2019.
Nicol, A., Carne, R., Gerstenberger, M., Christopersen, A., 2011. Induced seismicity and its implications for CO2 storage risk. Energy Proc. 4, 3699–3706.
Nicol, A., Seebeck, H., Field, B., McNamara, D., Childs, C., Craig, J., Rolland, A., 2017. Fault permeability and CO2 storage. 13th International Conference on Greenhouse Gas Control Technologies, GHGT-13, 14-18 November 2016, Lausanne, Switzerland. Energy Proc. 114 (2017), 3229–3236.
Nussbaum, C. and Bossart, P. (2004). Compilation of K-values from packer tests in the Mont Terri rock laboratory. Mont Terri Technical Note, TN 2005-10, p 29. Federal Office of Topography (swisstopo), Wabern, Switzerland.
Nussbaum, C., Bossart, P., Amann, F., Aubourg, C., 2011. Analysis of tectonic structures and excavation induced fractures in the Opalinus Clay, Mont Terri underground rock laboratory (Switzerland). Swiss J. Geosci. 104 (2011), 187–210.
Orellana, L.F., Giorgetti, C., Violay, M., 2019. Contrasting mechanical and hydraulic properties of wet and dry fault zones in a proposed shale-hosted nuclear waste repository. Geophys. Res. Lett. 46, 1357–1366. https://doi.org/10.1029/2018GL080384.
Payre, X., Maisons, C., Marblé, A., Thibeau, S., 2014. Analysis of the passive seismic monitoring performance at the Rousse CO2 storage demonstration pilot. Energy Proc. 63, 4339–4357.
Raleigh, C.B., Healy, J.H., Bredehoeft, J.D., 1976. An experiment in earthquake control at Rangely. Colorado. Science 191, 1230–1237.
Räss, L., Simon, N.S.C., Podladchikov, Y.Y., 2018. Spontaneous formation of fluid escape pipes from subsurface reservoirs. Nat. Sci. Rep. 8 (2018), 11116. https://doi.org/10.1038/s41598-018-29485-5.
Rybacki, E., Meier, T., Dresen, G., 2016. What controls the mechanical properties of shale rocks? – Part II: brittleness. J. Pet. Sci. Eng. 144, 39–58.
Rice, J.R., 1992. Fault stress states, pore pressure distributions, and the weakness of the San Andreas fault. In: Evans, B., Wong, T.-F. (Eds.), Fault Mechanics and Transport Properties in Rocks. Academic Press, London, UK, pp. 475–503, 144, 39-58.
Rinaldi, A.P., Rutqvist, J., Cappa, F., 2014a. Geomechanical effects on CO2 leakage through fault zones during large-scale underground injection. Int. J. Greenh. Gas Control 20 (2014), 117–131.
Rinaldi, A.P., Jeanne, P., Rutqvist, J., Cappa, F., Guglielmi, Y., 2014b. Effects of fault-zone architecture on earthquake magnitude and gas leakage related to CO2 injection in a multilayered sedimentary system. Greenh. Gas Sci. Technol. 4 (1), 99–120, 2014b.
Ruina, A.L., 1983. Slip instability and state variable friction laws. J. Geophys. Res. 88 (10), 359–10, 370.
Rutter, E.H., Hackston, A. (2017). Philosophical Transactions of the Royal Society of London, 375, 10.1098/rsta.2016.0001.
Rutter, E.H., Mecklenburgh, J., 2018. Influence of normal and shear stress on the hydraulic transmissivity of thin cracks in a tight quartz sandstone, a granite, and a shale. J. Geophys. Res. 123 https://doi.org/10.1002/2017JB014858.
Rutqvist, J., Graupner, B., Guglielmi, Y., Kim, T., Maßmannd, J., Son, T., Park, N., Shiu, J.-W., Urpi, W., Yoon, L., Ziefle, J.S., Birkholzer, G.J., 2020. An international model comparison study of controlled fault activation experiments in argillaceous claystone at the Mont Terri Laboratory. Int. J. Rock Mech. Min. Sci. 136, 104505. December 2020.
Rutqvist, J., Rinaldi .P., A., Cappa, F., Jeanne, P., Mazzoldi, A., Urpi, L., Guglielmi, Y., Vilarrasa, V., 2016. Fault activation and induced seismicity in geological carbon storage: lessons learned from recent modeling studies. J. Rock Mech. Geotech. Eng. 8 (6), 789–804. https://doi.org/10.1016/j.jrmge.2016.09.001, 2016ISSN 1674-7755.
Scibeck, J., Gleeson, T., MCKenzie, J.M., 2016. The biases and trends in fault zone hydrogeology conceptual models: global compilation and categorical data analysis. Geofluids 16 (2016), 782–798. https://doi.org/10.1111/gfl.12188.
Seebeck, H., Nicol, A., Walsh, J.J., Childs, C., Beetham, R.D., Pettinga, J., 2014. Fluid flow in fault zones from an active rift. J. Struct. Geol. 62, 52–64.
Segall, P., Rice, J.R., 1995. Dilatancy, compaction, and slip instability of a fluid-infiltrated fault. J. Geophys. Res. 100, 22155–22171.
Shapiro, S.A., Rothert, E., Rindschwentner, J., Rath, V., 2002. Characterization of fluid transport properties of reservoirs using induced microseismicity. Geophysics 67, 212–220.
Thoeny, R., 2014. Geomechanical analysis of excavation-induced rock mass behavior of faulted opalinus clay at the Mont Terri underground rock laboratory (Switzerland). Thesis. Engineering Geology Geological Institute ETH Zurich Sonneggstrasse.
Townend, J., Zoback, M., 2000. How faulting keeps the crust strong. Geology 28 (5), 399–402. May 20004 figures; 1 table.
Vannucchi, P., 2020. Scaly fabric and slip within fault zones. Geosphere 15 (2), 342–356.
Verdon, J.P., Stork, A.L., 2016. Carbon capture and storage, geomechanics and induced seismic activity. J. Rock Mech. Geotech. Eng. 8, 928–935.
Vidale, J.E., Shearer, P.M., 2006. A survey of 71 earthquake bursts across southern California: exploring the role of pore fluid pressure fluctuations and aseismic slip as drivers. J. Geophys. Res. 111, B05312. https://doi.org/10.1029/2005JB004034.
Vilarrasa, V., Carrera, J., 2015. Geologic carbon storage is unlikely to trigger large earthquakes and reactivate faults through which CO2 could leak. P. Natl. Acad. Sci. USA 112, 5938–5943. https://doi.org/10.1073/pnas.1413284112, 2015.
Viesca, R.C., Rice, J.R., 2012. Nucleation of slip-weakening rupture instability in landslides by localized increase of pore pressure. J. Geophys. Res. 117, B03104. https://doi.org/10.1029/2011JB008866.
Wenning, Q.C., Madonna, C., Zappone, A., Grab, M., Rinaldi, A.P., Plotze, M., Nussbaum, C., Giardini, D., Wiemer, S., 2021. Shale fault zone structure and stress dependent anisotropic permeability and seismic velocity properties (Opalinus Clay, Switzerland). J. Struct. Geol. 144, 104273.
White, J.A., Foxall, W., 2016. Assessing induced seismicity risk at CO2 storage projects: recent progress and remaining challenges. Int. J. Greenh. Gas Control 49, 413–424.
Wibberley, C.A.J., Yielding, G., Di Toro, G., 2008. Recent advances in the understanding of fault zone internal structure; a review. In: Wibberley, C.A.J., Kurz, W., Imber, J., Holdsworth, R.E., Collettini, C. (Eds.) (Ed.), Structure of Fault Zones: Implications for Mechanical and Fluid-flow Properties. Geological Society of London Special Publication, pp. 5–33 vol. 299.
Wu, W., Julia, S., Reece, J.S., Gensterblum, Y., Zoback, M.D., 2017. Permeability evolution of slowly slipping faults in shale reservoirs. Geophys. Res. Lett. 44, 10.1002/2017GL075506.
Wynants-Morel, N., Cappa, F., De Barros, L., Ampuero, J.-.P., 2020. Stress perturbation from aseismic slip drives the seismic front during fluid injection in a permeable fault. J. Geophys. Res. 125 https://doi.org/10.1029/2019JB019179 e2019JB019179.
Yeo, I.W., Brown, M.R.M., Ge, S., Lee, K.K., 2020. Causal mechanism of injection-induced earthquakes through the Mw 5.5 Pohang earthquake case study. Nat. Commun. 11, 2614. https://doi.org/10.1038/s41467-020-16408-0, 2020.
Yu, C., Matray, J.M., Goncalves, J., Jaeggi, D., Grasle, W., Wieczorek, K., Vogt, T., Sykes, E., 2017. Comparative study of methods to estimate hydraulic parameters in the hydraulically undisturbed Opalinus Clay (Switzerland). Swiss J. Geosci. 110, 85–104. https://doi.org/10.1007/s00015-016-0257-9.
Zappone, A., Rinaldi, A.P., Grab, M., Wenning, Q.C., Roques, C., Madonna, C., Obermann, A.C., Bernasconi, S.M., Brennwald, M.S., Kipfer, R., Soom, F., Cook, P., Guglielmi, Y., Nussbaum, C., Giardini, D., Mazzotti, M., Wiemer, Stefan, 2021. Fault sealing and caprock integrity for CO2 storage: an in situ injection experiment. Solid Earth 12, 319–343. https://doi.org/10.5194/se-12-319-202, 2021.
Zoback, M.D., Gorelick, S.M., 2012. Earthquake triggering and large-scale geologic storage of carbon dioxide. Proc. Natl Acad. Sci. 109 (26), 10164–10168. https://doi.org/10.1073/pnas.1202473109. June 26, 2012.
Zoback, M., Kohli, A., Das, I., McClure, M., 2012. The importance of slow slip on faults during hydraulic fracturing stimulation of shale gas reservoirs. SPE 155476. In: Americas Unconventional Resources Conference. Pittsburgh, Pennsylvania, USA, 5–7 June 2012.